
Increasing the Classification Margin with Uncertainty Driven Perturbations

Matteo Pagliardini¹ Gilberto Manunza¹ Martin Jaggi¹ Michael I. Jordan² Tatjana Chavdarova²

Abstract

Recently Shah et al., 2020 pointed out the pitfalls of the *simplicity bias*—the tendency of gradient-based algorithms to learn simple models—which include the model’s high sensitivity to small input perturbations, as well as sub-optimal margins. In particular, while Stochastic Gradient Descent yields max-margin boundary on linear models, such guarantee does not extend to non-linear models. To mitigate the simplicity bias, we consider uncertainty-driven perturbations (UDP) of the training data points, obtained iteratively by following the direction that maximizes the model’s estimated uncertainty. The uncertainty estimate does not rely on the input’s label and it is highest at the decision boundary, and—unlike loss-driven perturbations—it allows for using a larger range of values for the perturbation magnitude. Furthermore, as real-world datasets have non-isotropic distances between data points of different classes, the above property is particularly appealing for increasing the margin of the decision boundary, which in turn improves the model’s generalization. We show that UDP is guaranteed to achieve the maximum margin decision boundary on linear models and that it notably increases it on challenging simulated datasets. For nonlinear models, we show empirically that UDP reduces the simplicity bias and learns more exhaustive features. Interestingly, it also achieves competitive loss-based robustness and generalization trade-off on several datasets. Our codebase is available here: github.com/mpagli/Uncertainty-Driven-Perturbations

1. Introduction

While neural networks can represent any function (Hornik et al., 1989) and large models perfectly “fit” the *training* data, a question arises if these models *generalize well* for

¹EPFL, Switzerland ²UC Berkeley, USA. Correspondence to: Matteo Pagliardini <matteo.pagliardini@epfl.ch>.

the task at hand, i.e., if the accuracy on data samples that were *not* used during the training is high. For safety critical applications, addressing this question is often complex as it involves assessing the biases of the given dataset (Bolkunov et al., 2016; Gebru et al., 2021; Shah et al., 2020), the inductive bias of the predefined model (Fukushima & Miyake, 1982; LeCun & Bengio, 1998; Botev et al., 2021), the implicit bias of the optimization method used to train the model (Neysshabur et al., 2015; Zhang et al., 2017), and their “interaction”. In this paper, we limit our focus to that of *given a training dataset and a predefined model*, improving the chances that the model generalizes well. In this aim, a useful concept is that of the *margin* of a classifier $\mathcal{C}_\omega : \mathbf{x} \mapsto \hat{\mathbf{y}}$, with $\mathbf{x} \in \mathbb{R}^d$ denoting a data sample of finite dataset $\{\mathbf{x}_i, \mathbf{y}_i\}_{i=1}^N$ drawn from the training data distribution p_d , $\hat{\mathbf{y}} \in \mathbb{R}^c$ its prediction for c possible classes, and $\omega \in \mathbb{R}^m$ the parameters of the model. We define the margin as the maximum of the margins of the single points $m = \max(m(\mathbf{x}_1), \dots, m(\mathbf{x}_N))$, where the margin $m(\mathbf{x}_i)$ of a point \mathbf{x}_i is defined as the smallest distance from it to a decision boundary \mathcal{B} , i.e., $m(\mathbf{x}_i) = \min_{\tilde{\mathbf{x}} \in \mathcal{B}} \|\mathbf{x}_i - \tilde{\mathbf{x}}\|$.

Stochastic Gradient Descent (SGD, Robbins & Monro (1951); Kiefer & Wolfowitz (1952); Bottou (2010))—and variants of it—is the *de facto* optimization method for training neural networks. Interestingly, on linearly separable datasets, SGD provably converges to the *maximum-margin* linear classifier (Soudry et al., 2018), thereby achieving a superior generalization performance. Unfortunately, Shah et al., 2020 rigorously showed that this propriety of SGD does *not* follow on non-linear models such as the commonly used neural network architectures. In particular, the authors consider a nonlinear neural network with three parameters and a dataset for which we know that achieving max-margin requires using *all* the input coordinates. The authors then show that the model effectively uses *only one* of the input space coordinates, since the two other parameters are close to 0 (see Thm. 1 of Shah et al., 2020). This phenomenon is referred to as the “simplicity bias”, i.e. “the tendency of standard training procedures such as SGD to find simple models”. While several works argue that the simplicity bias can act as a form of regularization forcing the boundary hyperplane to be “simpler” and thus improve the generalization (Arpit et al., 2017; Dziugaite & Roy, 2017), others argue that in general, obtaining the simplest model can cause

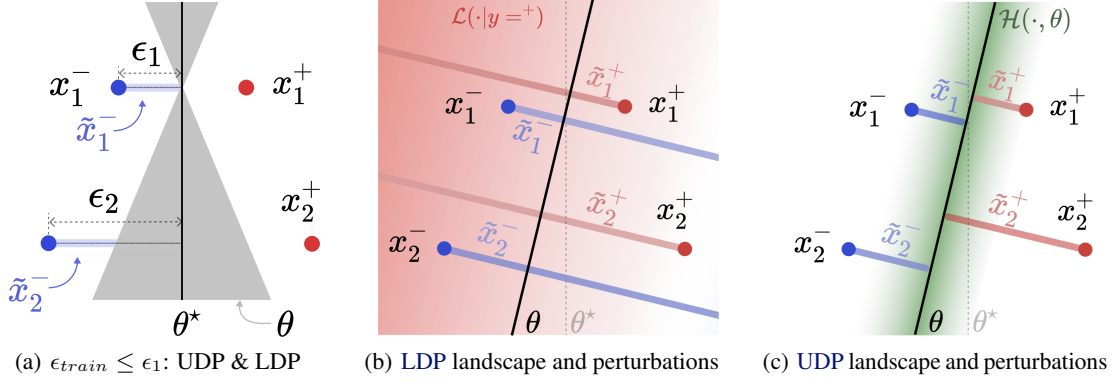


Figure 1: Pictorial representations of LDP and UDP. Circles represent training samples, and color their class $y \in \{-, +\}$. θ and θ^* denote the current decision boundary and the optimal one, resp. **Fig. (a)**. Given *ideal* data-perturbation training procedure using $\epsilon_{train} < \epsilon_1$ the perturbed data points (either with UDP or LDP) will belong to the shaded blue area (assuming the boundary θ has 0 training loss). Thus, the final decision boundary will belong to the shaded grey area, and we *cannot* guarantee the margin is maximized—see § 1. For clarity, only the perturbations \tilde{x}^- of the negative (blue) class are shown. **Fig. (b)** illustrates what is happening for LDP when ϵ is potentially large. The loss used for LDP perturbations (of positive samples) keeps increasing the further we go on the left of θ . For clarity, only the loss landscape of *positive* samples is shown, where darker is higher. In **Fig. (c)**, we see *why UDP’s property of not crossing the boundary is advantageous*. The green shade depicts the uncertainty, where darker is higher – starting from a point with negative label the uncertainty increases, reaches its maximum, and then decreases. Thus, the LDP and UDP perturbed samples—obtained by iteratively following the direction that *maximizes* these quantities—differ, and their possible regions are shown in red and blue shade, resp. for the positive and negative class. When the perturbed samples from the positive class pass θ^* , LDP yields training pair (\tilde{x}_i^+, y_i) with a semantically wrong label. This indicates that to avoid oscillations (caused by wrongly labeling input space regions), for LDP we are restricted to using $\epsilon_{train} \leq \epsilon_1$, but as Fig. (a) shows, this can be restrictive. On the other hand, for UDP we can have relatively larger ϵ which “locally adapts” and is effectively smaller in some region and larger in others. See § 4 for discussion.

it to falsely rely on *spurious* features (see Wang & Jordan, 2021, and references therein) and thus it may generalize poorly. Other examples where the simplicity bias is adverse include the related fields of *transfer learning* (Yosinski et al., 2014; Wang et al., 2020; Shafahi et al., 2020) and *distributional shift* (Sun et al., 2016; Amodei et al., 2016; Wang et al., 2020) where “exhaustive” features are required for good performances on the transfer task.

In addition, the hypothesis that simplicity bias aids generalization does not support the evidence that small perturbations added to the input can easily “fool” well-performing DNNs into making wrong predictions (Biggio et al., 2013; Szegedy et al., 2014)—referred to as robustness to perturbations. This observation motivated an active line of research on *adversarial training* (see Biggio & Roli, 2018, and references therein). AT methods exploit the prior knowledge for some applications, that all data points \tilde{x} within a small region around a training data point $x_i, i \in [1, N]$ belong to the same class:

$$\begin{aligned} \|\tilde{x} - x_i\| \leq \epsilon &\Rightarrow \tilde{y} = y_i, \quad \text{and} \quad \nexists j \in [1, N], \\ \text{s.t.} \quad j \neq i, y_j \neq y_i, \|\tilde{x} - x_j\| &\leq \epsilon. \end{aligned} \quad (\text{AT-Asm})$$

Starting from a training datapoint x_i , AT methods *iteratively* find a perturbation $\tilde{x}_i^0 \triangleq x_i$ using the loss of the classifier $\mathcal{L}(C_\omega(x_i^j), y_i), j = 0, \dots, k$ as an objective by following the direction that *maximizes* it, see § 2—herein called *loss-driven perturbations* (LDP). Popular such methods are *projected gradient descent* (PGD, Madry et al., 2018)—where the inner maximization step is implemented with k gradient ascent steps, and its “fast variants”—which take only one step to compute the perturbation δ , e.g., *fast gradient sign method* (FGSM, Goodfellow et al., 2015), see § 2. However, further empirical studies show that LDP methods often reduce the average accuracy on “clean” unperturbed test samples, indicating the two objectives—robustness and clean accuracy—might be competing (Tsipras et al., 2019; Su et al., 2018), and (Bubeck et al., 2021) provide conjecture on the inherent trade-offs between the size of a two-layer neural network and its robustness. Finally, (Zhang et al., 2019) show that learning models are vulnerable to small adversarial perturbations because the probability that data points lie around the decision boundary of the model is high (Zhang et al., 2019). In this work, we argue that the problems of poor robustness and high simplicity bias are related and that these can be improved by increasing the

margin of the decision boundary.

A separate line of work aims at increasing the interpretability of the model by associating to each of its predictions an *uncertainty estimate* (Kim et al., 2016; Doshi-Velez & Kim, 2017). Two main uncertainty types in machine learning are considered: (i) *aleatoric*—describing the *noise* inherent in the observations, as well as (ii) *epistemic*—uncertainty originating *from the model*. While the former *cannot* be reduced, the latter arises due to insufficient data to train the model, and it *can* be explained away given enough data (assuming access to universal approximation function). In the context of classification, apart from capturing high uncertainty due to overlapping regions of different classes, the epistemic uncertainty also captures which regions of the data space are not “visited” by the training samples. Importantly, as *many* functions can perfectly fit the training data—i.e. the function represented by the DNN model is often non-identifiable (Raue et al., 2013; Martín & González, 2010; Moran et al., 2021), and given an input \tilde{x} the uncertainty estimate incorporates quantification if possible hypothesis function “agree” on the prediction of \tilde{x} . It is thus natural to consider that training with perturbations that *maximize* this quantity will most efficiently narrow down the hypothesis set, leaving out the functions that increase the margin.

In summary, (i) a promising approach of incorporating inductive bias for improved generalization in training procedure is to use the prior knowledge that the label in the region around the training data points does not change; and on a separate note (ii) the epistemic uncertainty quantifies “how much the modeler sees a possibility to reduce its uncertainty by gathering more data” (Der Kiureghian & Ditlevsen, 2009). Moreover, since the former yields infinite training datasets, it is necessary to use efficient “search” of perturbations. Given these considerations, and in aim to improve the generalization of the neural networks, a natural question that arises is:

- *Can we use the direction of maximum uncertainty estimates to guide the search for efficient input-data perturbations? If yes, are there advantages over loss-driven perturbations?*

Since the quantitative methods yielding uncertainty estimates for neural networks are differentiable, we answer the former question affirmatively. In this paper, we consider “uncertainty driven perturbations” (UDP)—an inductive bias training framework that uses the model’s estimated estimates to find effective perturbations of the training samples.

Contributions. Our contributions can be summarized as:

- We first show that LDP suffers from high hyperparameter sensitivity of ϵ : (i) small ϵ may lead to reduced generalization, and (ii) large ϵ to unstable training and reduced test accuracy.

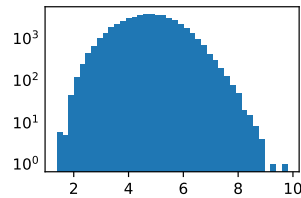


Figure 2: Histogram of Euclidean distances in input space for CIFAR-10 training samples to their closest neighbour of *opposite class*. That is, for each data sample x_i , we take the 1-nearest neighbour of different class x_j , with $y_i \neq y_j$, and we compute their distance. See § 3 for discussion.

- We propose uncertainty-driven perturbations (UDP) as a general family of algorithms that use the model’s uncertainty estimate for finding efficient perturbations of the training data samples. We show analytically that UDP converges to the max-margin for a simplistic linear setting, on which LDP does not. We further provide geometrical intuition on the advantages of UDP—namely, UDP reduces the ϵ -sensitivity relative to LDP.
- Empirically, we show that (i) albeit not trained explicitly, UDP is also robust to loss-based perturbations of the test sample, while maintaining a competitive trade-off with generalization on Fashion-MNIST, CIFAR-10, and SVHN (ii) it reduces the simplicity bias—as shown by the transferability of the features learned on CIFAR-10 to CIFAR-100, as well as (iii) it improves the generalization in low data regime when using latent space perturbations.

Structure. The background above, along with the preliminaries in § 2 suffice for the remaining of the paper. As this work is related to several relevant lines of works, a more extended overview is deferred to App. A, due to space constraints. Following the preliminaries, we (i) list motivating examples on the failure cases of LDP 3, (ii) formulate the proposed method, discuss its convergence and advantages in § 4, and (iii) empirical results are listed in § 5.

2. Preliminaries

Training with perturbations. In this section, we consider the supervised setting for simplicity. The perturbations can be applied in either the input space $\mathcal{X} \triangleq \mathbb{R}^d$ or the latent space of the model $\mathcal{C}_\omega(\cdot)$, i.e., $\mathcal{Z} \triangleq \mathbb{R}^l$, with l denoting the dimension of the latent space:

$$\min_{\omega} \mathbb{E}_{(x,y) \sim p_d} [\mathcal{L}(\mathcal{C}_\omega(\mathcal{E}(x) + \delta), y)], \quad (\text{ERM-P})$$

where the encoder \mathcal{E} is the identity when perturbations are applied in the input space, and \mathcal{L} denotes the loss function. For the latter, with abuse of notation, the model can be seen

as having an encoder part $\mathcal{E} : \mathbf{x} \mapsto \mathbf{z}$ and a classification part $\mathcal{C}_\omega : \mathbf{z} \mapsto \mathbf{y}$, and in that case $\delta \in \mathbb{R}^l$.

Loss Driven Perturbations (LDP). Common adversarial training methods *greedily* target the robustness weakness of DNNs by using *loss*-driven perturbations which find $\delta \triangleq \delta_\ell$ as follows:

$$\delta_\ell = \max_{\delta \in \Delta} \mathcal{L}(\mathcal{C}_\omega(\mathcal{E}(\mathbf{x}) + \delta), \mathbf{y}), \quad (\text{LDP})$$

where the added *worst-case* perturbation $\delta \in \mathbb{R}^d$ is constrained to a small region around the sample \mathbf{x} , typically $\Delta \triangleq \{\delta \text{ s.t. } \|\delta\|_k < \epsilon\}$ with $\epsilon > 0$, and $k \in \{1, 2, \infty\}$.

Common perturbation-search methods. The (LDP) maximization problem can be implemented in several ways. As in general the optimization is non-convex, [Lyu & Liang \(2015\)](#) propose approximating the inner maximization problem with Taylor expansion and then applying a Lagrangian multiplier. For ℓ_∞ -bounded attacks, this linearization yields the FGSM ([Goodfellow et al., 2015](#)) method:

$$\delta_{\text{FGSM}} \triangleq \epsilon \cdot \text{Sign}\left(\nabla_{\mathbf{x}} \mathcal{L}(\mathcal{C}_\omega(\mathbf{x}), \mathbf{y})\right), \quad (\text{FGSM})$$

where $\text{Sign}(\cdot)$ denotes the sign function. The PGD method ([Madry et al., 2018](#)) applies FGSM for $i = 1, \dots, k$ steps (with $\delta_{\text{PGD}}^0 \triangleq \mathbf{0}$):

$$\delta_{\text{PGD}}^i \triangleq \Pi_{\|\cdot\|_\infty \leq \epsilon} \left(\delta_{\text{PGD}}^{i-1} + \alpha \cdot \text{Sign}\left(\nabla_{\mathbf{x}} \mathcal{L}(\mathcal{C}_\omega(\mathbf{x} + \delta_{\text{PGD}}^{i-1}), \mathbf{y})\right) \right), \quad (\text{PGD})$$

where $\alpha \in [0, 1]$ is selected step size, and Π is projection on the ℓ_∞ -ball. PGD with k steps is often referred to as PGD- k . See also [App. A.3](#) for additional methods.

Training with $f(\tilde{\mathbf{x}}, \cdot)$ regularizer. Instead of using solely the perturbed samples during training, ([Zhang et al., 2019](#)) propose to use these for a regularization term to encourage smoothness of the output around the training samples:

$$\min_{\omega} \mathbb{E}_{(\mathbf{x}, \mathbf{y}) \sim p_d} \left[\mathcal{L}(\mathcal{C}_\omega(\mathbf{x}), \mathbf{y}) + \lambda \max_{\delta \in \Delta} \mathcal{L}(\mathcal{C}_\omega(\mathbf{x}), \mathcal{C}_\omega(\mathbf{x} + \delta)) \right], \quad (\text{TRADES})$$

where $\lambda \in (0, 1)$. The perturbation $\tilde{\mathbf{x}}$ is found such that the model’s output for it disagrees with the output for the training point \mathbf{x} as much as possible, and training aims to smoothen the output of $\mathcal{C}_\omega(\cdot)$ locally around \mathbf{x} .

Uncertainty estimation. For brevity, here we focus on the uncertainty estimation methods relevant for the remaining of the main paper, see [App. A](#) for a more extensive overview. Given an ensemble of M models $\{\mathcal{C}_\omega^{(m)}\}_{m=1}^M$ (for example, trained independently or sampled with MC Dropout ([Gal & Ghahramani, 2016](#)), see [App. A](#)) where each model outputs non-scaled values—“logits”, we define $\hat{\mathbf{y}} \in \mathbb{R}^C$ as the average prediction: $\hat{\mathbf{y}} = \frac{1}{M} \sum_{m=1}^M \text{Softmax}(\mathcal{C}_\omega^{(m)}(\mathbf{x}))$. Given $\hat{\mathbf{y}}$, there are several ways to estimate the model’s uncertainty, see ([Gal, 2016, §3.3](#)). In the remaining, we use the *entropy*

of the output distribution (over the classes) to quantify the uncertainty estimate of a given sample \mathbf{x} :

$$\mathcal{H}(\mathbf{x}, \omega) = - \sum_{c \in C} \hat{y}_c \log \hat{y}_c. \quad (\text{E})$$

3. Motivating examples

We consider two binary classification datasets in 2D, depicted in [Fig. 3](#), see [App. D](#) for additional datasets. Inspired from that of ([Zhang et al., 2019](#)), we design a dataset that has non-isotropic distances between the classes, i.e., the distance of the training samples to the optimal decision boundary increases from bottom left to top-right, which we name as the *Narrow Corridor* (NC) dataset. The other dataset is that of ([Shah et al., 2020](#)) called *linear & multiple 5-slabs* (LMS-5), which is challenging because a single feature (the x -coordinate) suffices to obtain 0 training loss, but the margin of such boundary is sub-optimal. The two datasets have in common that the standard training *fails* to learn a decision boundary with a good margin—see first column in [Fig. 3](#), which motivates training with input perturbations. From the top row of [Fig. 3](#) we observe that satisfying *AT-Asm* “globally” is restrictive for the NC dataset and LDP training both for TRADES and PGD: (i) choosing an ϵ_{train} that does not violate this assumption gives sub-optimal decision boundary in the top-right corner, and on the other hand (ii) selecting value for ϵ_{train} that violates *AT-Asm* only in some small regions (in bottom-left) causes miss-classifying the *training* samples in that region. In the presence of strong tendency toward the simplicity bias phenomenon—bottom row of [Fig. 3](#) we observe LDP has limited capacity to improve the decision boundary—as shown in ([Shah et al., 2020](#)).

Relevance for real-world datasets. [Fig. 2](#) shows the distances between the closest data samples of opposite class on CIFAR-10 in input space, where we observe that these distances are non-isotropic. In particular, choosing an ϵ_{train} that satisfies the *AT-Asm* is restrictive: there exist a large mass of data samples between which we can not guarantee the margin will be satisfactory after training with perturbations. On the other hand, when training with a larger ϵ —as demonstrated in this section—LDP can have undesirable behavior such as low accuracy in the region where *AT-Asm* is violated, or oscillations—see also [Fig. 8\(d\)](#)—making the training inefficient. Since the margin and data points distances in input space are positively correlated to those in the latent space—see ([Sokolich et al., 2017](#)), this indicates that the ϵ -sensitivity of LDP may be relevant for real-world datasets.

4. Uncertainty Driven Perturbations

We propose *Uncertainty Driven Perturbations* (UDP) which method, as the name implies, aims at finding perturbations

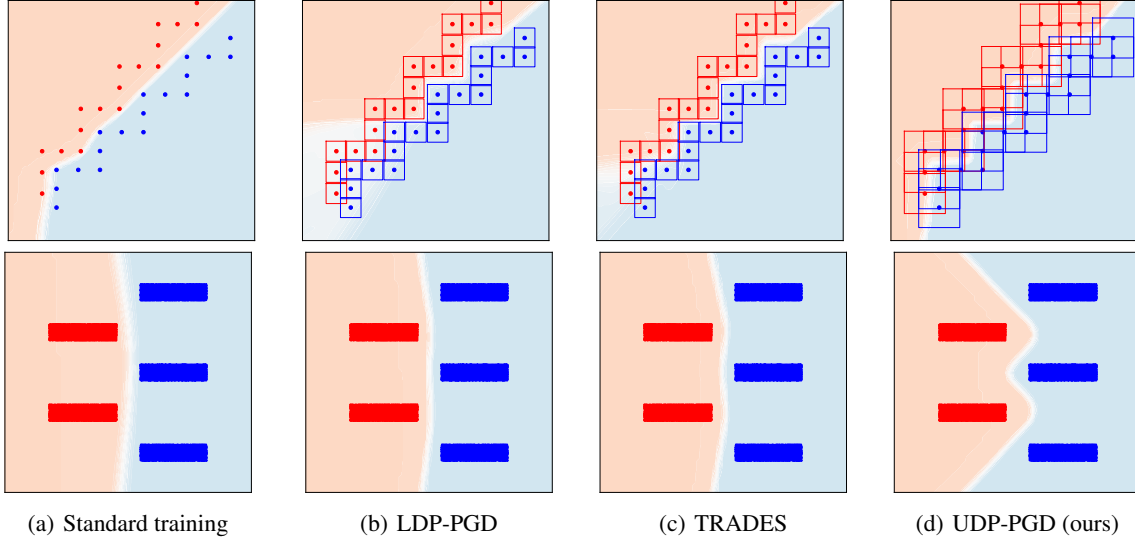


Figure 3: Standard, LDP-PGD, TRADES and UDP training shown in first to fourth column, resp.; on the *Narrow Corridor* and the *LMS-5* datasets—see § 3, where their color represents the class, and the background the decision boundary after converging. **Top row.** On the NC dataset we observe that (i) standard training obtains decision boundary which passes close to the training data points, (ii) LDP-PGD and TRADES fail in regions where ϵ_{train} violates the *AT-Asm* assumption locally (iii) UDP-PGD despite using an ϵ twice as large, can recover a boundary close to the max-margin. **Bottom row.** On *LMS-5*, training with LDP-PGD or TRADES using the largest possible ϵ under assumption *AT-Asm* is not enough to recover the max-margin boundary decision. UDP with a large ϵ , however, retrieves the optimal boundary. See § 3 for discussion.

that maximize the model’s uncertainty estimate as follows:

$$\delta_u = \arg \max_{\delta \in \Delta} \mathcal{H}(\mathcal{E}(x) + \delta, \omega), \quad (\text{UDP})$$

where we use same notation as for (LDP), to include the possibility for latent-space perturbations—see § 2. When using a *single model* ($M = 1$), UDP can be seen as *maximum entropy perturbations*.

4.1. Uncertainty Driven Perturbations (UDP)

Similar to loss-based *ERM-P*, the inner maximization of *UDP*—for both image and latent-space perturbations—can be implemented analogously to *PGD* and *FGSM* as follows (with $\delta_{\text{PGD}}^0 \triangleq \mathbf{0}$):

$$\delta_u^i \triangleq \underset{\|\cdot\|_\infty \leq \epsilon}{\text{arg max}} \left(\delta_{\text{UPD}}^{i-1} + \alpha \cdot \text{Sign} \left(\nabla_x \mathcal{H}(\mathcal{E}(x) + \delta_{\text{UPD}}^{i-1}, \omega) \right) \right). \quad (\text{UDP-PGD})$$

Inspired from (Zhang et al., 2019), we also define a variant of *UDP* which does *UDP* training with regularization term (*UDPR*) as follows:

$$\min_{\omega} \mathbb{E}_{(x, y) \sim p_d} \left[\mathcal{L}(\mathcal{C}_\omega(x), y) + \lambda \mathcal{L}(\mathcal{C}_\omega(x + \delta_u), y) \right], \quad (\text{UDPR})$$

with $\lambda \in (0, 1)$, and δ_u as in *UDP*. To show convergence on linear models, it is necessary that the perturbed samples \tilde{x}_i are distributed between the original data points x_i , see § 4.2. Rather than running the maximization for k steps—as

per (*PGD*) and then project back in a way that makes \tilde{x}_i uniformly distributed over the iterations, it is more computationally efficient to instead sample the number of steps uniformly in the interval $(1, k - 1)$ at each iteration, and for each sample. Alg. 1 summarizes the details of the two variants, where for simplicity, we use a single model $M = 1$.

4.2. On the convergence of UDP

Setting. Consider a setting of binary classification of $x \in \mathbb{R}^d$ data samples, sampled from the data distribution p_d which represents a mixture of two Gaussians with means μ^1, μ^2 (with $\mu^1 < \mu^2$), with corresponding label $y^1 = -1$ and $y^2 = +1$. For this problem, the optimal boundary is at $\omega^* = 0$. Since *SGD* yields the max-margin classifier for this setting (and so does regular training—see § 1), to represent more closely non-linear systems we consider a weaker assumption for the optimizer: at each iteration n , given data points \tilde{x}_n^1 and $\tilde{x}_n^{(2)}$, an oracle returns a *direction* $\tilde{\omega}_n$ that belongs in the interval between \tilde{x}_n^1 and $\tilde{x}_n^{(2)}$, that is:

$$\exists \alpha_n \in (0, 1), \quad \text{s.t.} \quad \tilde{\omega}_n = \alpha_n \tilde{x}_n^1 + (1 - \alpha_n) \tilde{x}_n^{(2)}, \quad (\text{S1})$$

where we assume:

$$\alpha_n \sim \mathcal{U}(0, 1), \quad \text{i.e.} \quad \mathbb{E}[\alpha] = \frac{1}{2}, \quad (\text{A1})$$

Given ω_n and $\tilde{\omega}_n$, the update rule is as follows:

$$\omega_{n+1} = \omega_n + \eta(\tilde{\omega}_n - \omega_n), \quad (\text{S2})$$

Algorithm 1 UDP pseudocode (in input space).

```

1: Input: Classifier  $C_{\omega_0}$  with logits output and initial
   weights  $\omega_0$ , stopping time  $T$ , data distribution  $p_d$ , learning
   rate  $\eta$ , its loss  $\mathcal{L}$ ,  $L_\infty$  ball radius  $\epsilon$ , perturbation
   step size  $\alpha$ , number of attack iterations  $K$ , Boolean
   flag–train with a regularizer reg, regularizer weight  $\gamma$ .
2: for  $t \in 0, \dots, T-1$  do
3:   Sample  $x, y \sim p_d$ 
4:    $\delta_u^0 \leftarrow \mathbf{0}$ 
5:   sample  $k \sim \mathcal{U}(1, K-1)$ 
6:   for  $i \in 0, \dots, k$  do
7:      $p \leftarrow \text{Softmax}(C_{\omega_t}(x + \delta_u^i))$ 
8:      $\mathcal{H} \leftarrow -\sum_c p_c \log(p_c)$  (Compute entropy)
9:      $\delta_u^{i+1} = \delta_u^i + \alpha \text{sign}(\nabla_{\delta_u^i} \mathcal{H})$ 
10:    Projection  $\delta_u^{i+1} \leftarrow \Pi_{\|\cdot\|_\infty \leq \epsilon} \delta_u^{i+1}$ 
11:  end for
12:  if reg is True then
13:     $\omega_{t+1} = \omega_t - \eta \nabla_\omega \mathcal{L}(C_{\omega_t}(x), y) - \gamma \nabla_\omega \mathcal{L}(C_{\omega_t}(x + \delta_u^K), y)$ 
14:  else
15:     $\omega_{t+1} = \omega_t - \eta \nabla_\omega \mathcal{L}(C_{\omega_t}(x + \delta_u^K), y)$ 
16:  end if
17: end for
18: Output:  $\omega_T$ 

```

where $\eta \in (0, 1)$ is the step-size.

Theorem 4.1 (Convergence towards the max-margin without ϵ dependence). *Given an oracle that takes as input two data points $\tilde{x}^{(1)}, \tilde{x}^{(2)} \in \mathbb{R}$ and returns a point that lies between these points sampled uniformly at random, the UDP method as per Alg. 1 in expectation tends to move towards the max-margin classifier on a linearly separable dataset.*

The proof is provided in App. B. Although the problem is simple and standard training converges to the max-margin solution, it is worth noting that LDP fails to converge if $\epsilon > |\frac{\mu_1 - \mu_2}{2}|$, in which case the trained classifier can have 0 accuracy, as the labels of the perturbed training samples are flipped. This shows that stopping at the current boundary is beneficial. Our illustrative examples with non-isotropic distances between different class samples, further illustrate why such sensitivity to ϵ is relevant.

Revisiting the 2D motivating examples. We observe from Fig. 3-(d) that by replacing the perturbation objective with the model’s estimated uncertainty we are able to use larger ϵ_{train} for the NC dataset, and interestingly we obtain a decision boundary (close to) the max-margin. Similarly, for the challenging high simplicity bias dataset in the second row, UDP achieves a decision boundary (close to) that of the max-margin—see Fig. 7. App. D provides the reader with additional insights how UDP works using additional datasets as well as a different uncertainty estimation model,

in particular one based on Gaussian Process (Rasmussen & Williams, 2005).

Additional advantages of UDP. UDP is *unsupervised*, as it does not use the ground truth labels y to compute the perturbations. As such, it can be used for unsupervised methods that output probability estimates. On the other hand, LDP relies on the class label of the starting training sample x_i , thus the loss increases towards the decision boundary and the further we are from x_i the larger it increases, see Fig. 1.

5. Experiments

As UDP is a general framework where the objective for finding perturbations is estimated uncertainty, we conduct several types of experiments to empirically verify if such an approach is promising for real world datasets as well. However, we do not aim to provide new state of art results in related fields, and in § 6 we list some open directions. Primarily, (i) given a fixed model capacity we compare the generalization-robustness trade-off of UDP in input and in latent space—see § 5.1, (ii) the model’s generalization with increasingly larger capacity—§ 5.2, and finally (iii) we estimate the simplicity bias by analyzing the transferability of the learned features from a source (CIFAR-10) to a different target domain (CIFAR-100) in § 5.3.

Datasets & models. We evaluate on Fashion-MNIST (Xiao et al., 2017), SVHN (Netzer et al., 2011), CIFAR-10 (Krizhevsky, 2009) and CIFAR-100 (Krizhevsky et al.). Throughout our experiments, we use two different architectures: LeNet (Lecun et al., 1998) for Fashion-MNIST, as well as ResNet-18 (He et al., 2016) for CIFAR-10 and SVHN. For all experiments in the main paper, we use a single model for UDP, for fair comparison with the baselines. See App. F for details on the implementation.

5.1. Robustness-generalization trade-off for fixed model

As UDP aims to increase the classification margin, l_p robustness may be a suitable test bench. Indeed, if the margin for a classifier C_ω is more than ϵ , then there are no perturbations $x + \delta$ constrained to $\|\delta\|_2 < \epsilon$ that can be found such that $C_\omega(x + \delta)$ crosses the boundary. Thus, we evaluate the l_2 as well as the l_∞ robustness for several datasets and ϵ_{test} . We also compute the robustness-generalization trade-off by averaging robust and clean accuracy. Results on catastrophic overfitting are available in App. E.

Methods & robustness evaluation. We compare: (i) **UDP**, (ii) **PGD** (Madry et al., 2018), and (iii) **TRADES** (Zhang et al., 2019), the latter two are described § 2. For all our l_∞ and l_2 -robustness values, we use the standard pipeline of *AutoAttack* (Croce & Hein, 2020), which considers four different attacks: APGD_{CE} , $\text{APGD}_{\text{DLR}}^T$, FAB^T , and Square.

Table 1: Results on CIFAR-10 and SVHN *without* data augmentation including best robust accuracy for l_∞ and l_2 as given by the AutoAttack standard pipeline, as well as the best trade-off between generalization and robustness given by averaging the clean and robust accuracy. For each method, the set of hyperparameters giving the best average l_∞ robustness between $\epsilon_{\text{train}} = 0.01$ and $\epsilon_{\text{train}} = 0.03$ is selected. The best scores along with all scores within standard deviation reach for each column are in bold. We observe how large ϵ_{train} tend to be selected for UDP methods.

		CIFAR-10			
		l_∞		l_2	
method		$\epsilon_{\text{test}} = 0.01$	$\epsilon_{\text{test}} = 0.03$	$\epsilon_{\text{test}} = 0.5$	$\epsilon_{\text{test}} = 1.0$
Best Robust Accuracy	TRADES ($\epsilon_{\text{train}} = 0.03$)	61.8 \pm 0.8	31.0 \pm 0.3	46.9 \pm 1.2	18.3 \pm 0.7
	PGD ($\epsilon_{\text{train}} = 0.02$)	62.7 \pm 0.5	31.2 \pm 0.3	47.4 \pm 0.6	17.9 \pm 0.5
	UDPR ($\epsilon_{\text{train}} = 0.05$)	64.9 \pm 0.4	31.1 \pm 0.3	50.2 \pm 0.5	19.1 \pm 0.4
	UDP-PGD ($\epsilon_{\text{train}} = 0.06$)	64.2 \pm 0.4	33.4 \pm 0.3	50.1 \pm 1.8	19.5 \pm 1.4
Best Trade-off	TRADES ($\epsilon_{\text{train}} = 0.02$)	71.3 \pm 0.4	54.9 \pm 0.4	63.4 \pm 0.8	47.6 \pm 0.2
	PGD ($\epsilon_{\text{train}} = 0.01$)	72.7 \pm 0.4	52.6 \pm 0.2	64.4 \pm 0.3	47.7 \pm 0.4
	UDPR ($\epsilon_{\text{train}} = 0.05$)	72.3 \pm 0.4	55.4 \pm 0.2	65.0 \pm 0.1	49.4 \pm 0.3
	UDP-PGD ($\epsilon_{\text{train}} = 0.04$)	73.1 \pm 0.6	55.7 \pm 0.8	65.8 \pm 0.3	48.9 \pm 0.3
		SVHN			
Best Robust Accuracy	TRADES ($\epsilon_{\text{train}} = 0.05$)	72.9 \pm 1.5	44.6 \pm 1.6	37.7 \pm 2.5	6.7 \pm 0.8
	PGD ($\epsilon_{\text{train}} = 0.04$)	75.7 \pm 0.2	43.3 \pm 0.4	30.5 \pm 1.0	5.5 \pm 0.1
	UDPR ($\epsilon_{\text{train}} = 0.05$)	79.7 \pm 0.1	40.3 \pm 1.4	34.4 \pm 1.5	6.1 \pm 0.8
	UDP-PGD ($\epsilon_{\text{train}} = 0.04$)	79.3 \pm 0.1	39.7 \pm 0.7	33.4 \pm 0.6	5.8 \pm 0.6
Best Trade-off	TRADES ($\epsilon_{\text{train}} = 0.05$)	79.4 \pm 1.2	65.2 \pm 0.3	61.8 \pm 0.8	46.3 \pm 0.1
	PGD ($\epsilon_{\text{train}} = 0.02$)	85.6 \pm 0.3	64.6 \pm 0.3	61.9 \pm 0.2	48.9 \pm 0.1
	UDPR ($\epsilon_{\text{train}} = 0.05$)	86.4 \pm 0.0	67.1 \pm 0.4	63.8 \pm 0.7	49.6 \pm 0.2
	UDP-PGD ($\epsilon_{\text{train}} = 0.04$)	86.5 \pm 0.1	66.7 \pm 0.4	63.6 \pm 0.2	49.8 \pm 0.2

5.1.1. INPUT SPACE

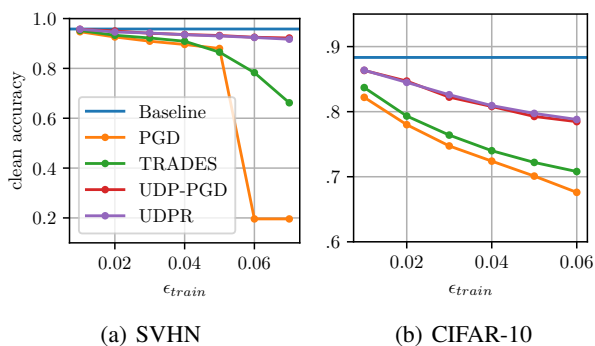


Figure 4: *Clean accuracy* (y -axis) comparison between PGD, TRADES, UDP-PGD, and UDPR on **SVHN** and **CIFAR-10**, for varying ϵ_{train} used for training (x -axis). Results are averaged over multiple runs. See § 5.1.

Setup. For TRADES, UDP, and PGD, we train several models with ϵ_{train} ranging from 0.01 to 0.08, all the perturbation at train time are obtained using the l_∞ norm. To find the perturbations, we used step sizes α ranging from 0.001 to 0.012 and a number of steps from 10 to 40. For the *AutoAttack* evaluation, we use $\epsilon_{\text{test}} \in \{0.01, 0.03\}$ for l_∞ -robustness and $\epsilon_{\text{test}} \in \{0.5, 1.0\}$ for l_2 -robustness.

Results. In Fig. 4, we compare the clean test accuracy of

PGD, TRADES and UDP-PGD on SVHN and CIFAR-10, see App. E for Fashion-MNIST. We *consistently* observe in all our experiments that the clean accuracy of UDP is is *consistently superior* to the one of LPD-PGD and TRADES, across varying ϵ_{train} . Tab. 1, 2 and 3 show that UDP methods offer competitive and often improved trade-off between robustness and accuracy, relative to LPD-PGD and TRADES, in terms of their robust accuracy as given by AutoAttack. We also show UDPR and UDP-PGD provide a better trade-off between robustness and clean accuracy. Those improvements are typically obtained for larger values of ϵ_{train} .

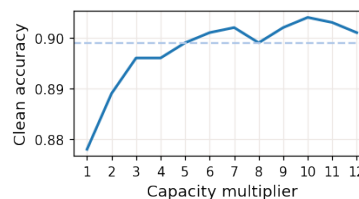


Figure 5: *Clean accuracy* (y -axis) comparison between models trained with UDP using $\epsilon = 0.1$, for varying capacity of the model (x -axis). Dashed line represents the clean accuracy of standard training and corresponds to model capacity 1—however, has $\sim 0\%$ robustness accuracy.

Table 2: AutoAttack robustness (top) and trade-off (bottom) on Fashion-MNIST, where for the latter we average the clean and robust accuracy. For each method, one set of hyperparameters is selected according to its mean l_∞ -robust accuracy over $\epsilon_{\text{test}} \in \{0.05, 0.1, 0.2\}$. Notice that the best scores for UDP are obtained for large ϵ_{train} —often 0.5—which clearly violates *AT-Asm*. Results are averaged over 3 seeds.

Best Robust Accuracy					
ϵ_{test}	clean	l_∞			l_2
	acc	0.05	0.1	0.2	1.5
PGD ($\epsilon_{\text{train}} .2$)	78.9	73.9	69.3	58.3	2.8
TRADES ($\epsilon_{\text{train}} .2$)	82.1	77.1	70.6	55.1	5.6
UDPR ($\epsilon_{\text{train}} .5$)	84.8	72.5	60.9	40.0	34.1
UDP-PGD ($\epsilon_{\text{train}} .5$)	82.3	74.9	66.8	49.6	27.5
Best Trade-off					
ϵ_{test}	acc	0.05	0.1	0.2	1.5
	PGD ($\epsilon_{\text{train}} .2$)	78.9	75.5	73.5	67.9
TRADES ($\epsilon_{\text{train}} .2$)	82.1	79.7	76.5	68.7	44.0
UDPR ($\epsilon_{\text{train}} .5$)	84.8	78.6	72.8	62.3	59.4
UDP-PGD ($\epsilon_{\text{train}} .3$)	84.2	80.2	75.6	65.4	53.7

Table 3: Results on CIFAR-10 *with* data augmentation. For each method, we trained models with l_∞ -norm and ϵ_{train} ranging from 0.01 to 0.08. We pick one model to display based on the best average l_∞ robustness on $\epsilon_{\text{test}} = 0.01$ and $\epsilon_{\text{test}} = 0.03$. We can observe how the best ϵ_{train} for UDP methods tends to be large. All robust accuracies are computed using the AutoAttack standard pipeline.

ϵ_{test}	clean	l_∞		l_2	
	acc	0.01	0.03	0.5	1.0
PGD ($\epsilon_{\text{train}} .03$)	83.8	72.9	47.6	58.5	25.5
UDPR ($\epsilon_{\text{train}} .05$)	83.4	74.1	45.3	58.5	25.5
UDP-PGD ($\epsilon_{\text{train}} .08$)	87.5	76.9	37.1	59.5	21.4

5.1.2. LATENT SPACE & LOW-DATA REGIME

We consider the low-data regime, to study if fewer samples suffice to learn a decision boundary that has a good margin between the considered training samples. As in (Yuksel et al., 2021) we take 5% of the training data of CIFAR-10. We apply the perturbations in the latent space of a ResNet-18 model by splitting it in an encoder part \mathcal{E} (up to the last convolutional layer) and a classifier part \mathcal{C}_ω (the rest of the network)—see *ERM-P*. Both the encoder and the classifier are trained jointly with perturbations, using $\epsilon = 0.2$, $\alpha = 0.01$ and 20 attack iterations. Tab. 5 indicates that the UDP methods lead to better clean accuracy, relative to LDP and TRADES.

Table 4: Feature transferability: features of CIFAR-10 pre-trained models (from Tab.1) are fixed, and we train a classifier on CIFAR-100 using their embeddings. See § 5.3.

method		transfer accuracy
baseline		42.5 \pm 0.3
Best	TRADES ($\epsilon_{\text{train}} = .03$)	42.7 \pm 0.1
Robust	PGD ($\epsilon_{\text{train}} = .02$)	42.6 \pm 0.1
Accuracy	UDP-PGD ($\epsilon_{\text{train}} = .06$)	45.3 \pm 0.3
Best	TRADES ($\epsilon_{\text{train}} = .02$)	43.1 \pm 0.3
Trade-off	PGD ($\epsilon_{\text{train}} = .01$)	43.3 \pm 1.2
	UDP-PGD ($\epsilon_{\text{train}} = .04$)	45.7 \pm 0.6

Table 5: Low-data regime comparison, with 5% of CIFAR-10 training set, and *latent-space* perturbations (*LS-* prefix).

method	clean accuracy
baseline	48.2 \pm 0.9
LS-PGD ($\epsilon_{\text{train}} = 2$)	37.3 \pm 0.3
LS-TRADES ($\epsilon_{\text{train}} = 2$)	46.9 \pm 0.3
LS-UDPR ($\epsilon_{\text{train}} = 2$)	53.1 \pm 0.9
LS-UDP-PGD ($\epsilon_{\text{train}} = 2$)	52.5 \pm 0.3

5.2. Increasingly large model capacity

In the previous section, we observed that the clean accuracy decreases for UDP as ϵ_{train} increases—although notably less than LDP. As pointed out by Madry et al. (2018), and recently shown by Bubeck et al. (2021) larger model capacity may be necessary for robustness. Thus, in this section, we increase the model capacity to observe if the test accuracy of UDP increases, see App. F.2 for implementation. From Fig. 5 we observe that this is indeed likely the case: with increased capacity, we outperform the clean training in terms of clean test accuracy, while having significantly improved robustness—see Tab. 2 for the corresponding robustness.

5.3. Estimating simplicity bias

To estimate if the simplicity bias is reduced—if the model maintains more exhaustive set of features, we use the embedding (while keeping it fixed) of the previously trained models on CIFAR-10, to train a model on CIFAR-100. Tab. 4 indicates that UDP has reduced simplicity bias.

6. Discussion

We proposed using the model’s estimated uncertainty as an objective to iteratively find perturbations of the input training samples called UDP. Moreover, we provided some geometrical explanations on the difference between loss-driven perturbations (LDP) around the decision boundary, and we showed that such an advantage allows UDP to use a potentially larger magnitude of perturbation. Our pre-

liminary, yet diverse, set of experiments showed that this approach is promising for real-world datasets as well.

We hope to initiate the study of the inherent trade-offs for varying perturbation schemes using online learning tools, to provide more rigorous bounds on the worst-case performance to any adversary. This tackles generalization in a broader sense, as relevant per safety-critical applications. On the empirical side, while we focused on single-model UDP for a fair comparison, it remains an interesting direction to explore UDP with different uncertainty estimation methods.

ACKNOWLEDGEMENTS

TC thanks the support by the Swiss National Science Foundation (SNSF), grant P2ELP2_199740. The authors thank Yixin Wang for insightful discussions and feedback.

References

- Amodei, D., Olah, C., Steinhardt, J., Christiano, P., Schulman, J., and Mané, D. Concrete problems in ai safety. *arXiv:1606.06565*, 2016.
- Andriushchenko, M. and Flammarion, N. Understanding and improving fast adversarial training. In *NeurIPS*, 2020.
- Arpit, D., Jastrzundebdski, S., Ballas, N., Krueger, D., Bengio, E., Kanwal, M. S., Maharaj, T., Fischer, A., Courville, A., Bengio, Y., and Lacoste-Julien, S. A closer look at memorization in deep networks. In *ICML*, pp. 233–242. JMLR, 2017.
- Biggio, B. and Roli, F. Wild patterns: Ten years after the rise of adversarial machine learning. *Pattern Recognition*, 84:317–331, 2018. ISSN 0031-3203. doi: <https://doi.org/10.1016/j.patcog.2018.07.023>.
- Biggio, B., Corona, I., Maiorca, D., Nelson, B., Šrndić, N., Laskov, P., Giacinto, G., and Roli, F. Evasion attacks against machine learning at test time. In *Machine Learning and Knowledge Discovery in Databases*, pp. 387–402, 2013. ISBN 978-3-642-40994-3.
- Blei, D. M., Kucukelbir, A., and McAuliffe, J. D. Variational inference: A review for statisticians. *Journal of the American Statistical Association*, 112(518):859–877, 2017.
- Bolukbasi, T., Chang, K.-W., Zou, J., Saligrama, V., and Kalai, A. Man is to computer programmer as woman is to homemaker? debiasing word embeddings. In *NIPS*, pp. 4356–4364, 2016.
- Botev, A., Jaegle, A., Wirnsberger, P., Hennes, D., and Higgins, I. Which priors matter? benchmarking models for learning latent dynamics. In *NeurIPS: Track on Datasets and Benchmarks*, 2021.
- Bottou, L. Large-scale machine learning with stochastic gradient descent. In *COMPSTAT*, 2010.
- Bubeck, S., Li, Y., and Nagaraj, D. A law of robustness for two-layers neural networks. In *COLT*, 2021.
- Croce, F. and Hein, M. Reliable evaluation of adversarial robustness with an ensemble of diverse parameter-free attacks. In *ICML*, pp. 2206–2216. PMLR, 2020.
- Cubuk, E. D., Zoph, B., Schoenholz, S. S., and Le, Q. V. Intriguing properties of adversarial examples, 2017.
- Der Kiureghian, A. and Ditlevsen, O. Aleatoric or epistemic? does it matter? *Structural Safety*, 31(2):105–112, 2009. ISSN 0167-4730. doi: [10.1016/j.strusafe.2008.06.020](https://doi.org/10.1016/j.strusafe.2008.06.020).
- Doshi-Velez, F. and Kim, B. Towards a rigorous science of interpretable machine learning. *arXiv:1702.08608*, 2017.
- Dziugaite, G. K. and Roy, D. M. Computing nonvacuous generalization bounds for deep (stochastic) neural networks with many more parameters than training data. In *Proceedings of the 33rd Annual Conference on Uncertainty in Artificial Intelligence (UAI)*, 2017.
- Elsayed, G. F., Krishnan, D., Mobahi, H., Regan, K., and Bengio, S. Large margin deep networks for classification. In *NeurIPS*, pp. 850–860, 2018.
- Fukushima, K. and Miyake, S. Neocognitron: A self-organizing neural network model for a mechanism of visual pattern recognition. In Amari, S.-i. and Arbib, M. A. (eds.), *Competition and Cooperation in Neural Nets*, pp. 267–285. Springer Berlin Heidelberg, 1982. ISBN 978-3-642-46466-9.
- Gal, Y. *Uncertainty in Deep Learning*. PhD thesis, University of Cambridge, 2016.
- Gal, Y. and Ghahramani, Z. Dropout as a Bayesian Approximation: Representing Model Uncertainty in Deep Learning. In *Proceedings of The 33rd International Conference on Machine Learning*, volume 48 of *Proceedings of Machine Learning Research*, pp. 1050–1059, 2016.
- Gebu, T., Morgenstern, J., Vecchione, B., Vaughan, J. W., Wallach, H., au2, H. D. I., and Crawford, K. Datasheets for datasets. *arXiv:1803.09010*, 2021.
- Goodfellow, I. J., Shlens, J., and Szegedy, C. Explaining and harnessing adversarial examples. In *ICLR*, 2015.
- Guo, C., Pleiss, G., Sun, Y., and Weinberger, K. Q. On calibration of modern neural networks. In *ICML*, 2017.

- He, K., Zhang, X., Ren, S., and Sun, J. Deep residual learning for image recognition. In *CVPR*, 2016.
- Hornik, K., Stinchcombe, M., and White, H. Multilayer feedforward networks are universal approximators. *Neural Networks*, 2(5):359–366, 1989. ISSN 0893-6080. doi: [https://doi.org/10.1016/0893-6080\(89\)90020-8](https://doi.org/10.1016/0893-6080(89)90020-8).
- Jaynes, E. T. Information theory and statistical mechanics. *Physical review*, 106:620–630, 1957. doi: 10.1103/PhysRev.106.620.
- Jospin, L. V., Buntine, W., Boussaid, F., Laga, H., and Bennamoun, M. Hands-on bayesian neural networks – a tutorial for deep learning users. *arXiv preprint arXiv:2007.06823*, 2021.
- Kiefer, J. and Wolfowitz, J. Stochastic Estimation of the Maximum of a Regression Function. *The Annals of Mathematical Statistics*, 23(3):462 – 466, 1952. doi: 10.1214/aoms/1177729392.
- Kim, B., Khanna, R., and Koyejo, O. O. Examples are not enough, learn to criticize! criticism for interpretability. In *NIPS*, volume 29, 2016.
- Kingma, D. P. and Ba, J. Adam: A method for stochastic optimization. In *ICLR*, 2015.
- Krizhevsky, A. Learning Multiple Layers of Features from Tiny Images. Master’s thesis, 2009.
- Krizhevsky, A., Nair, V., and Hinton, G. Cifar-100 (canadian institute for advanced research). URL <http://www.cs.toronto.edu/~kriz/cifar.html>.
- Lakshminarayanan, B., Pritzel, A., and Blundell, C. Simple and Scalable Predictive Uncertainty Estimation Using Deep Ensembles. In *Proceedings of the 31st International Conference on Neural Information Processing Systems*, pp. 6405–6416, Red Hook, NY, USA, 2017. Curran Associates Inc.
- Larsen, A. B. L., Sønderby, S. K., and Winther, O. Autoencoding beyond pixels using a learned similarity metric. In *ICML*, 2016.
- LeCun, Y. and Bengio, Y. *Convolutional Networks for Images, Speech, and Time Series*, pp. 255–258. MIT Press, Cambridge, MA, USA, 1998. ISBN 0262511029.
- Lecun, Y., Bottou, L., Bengio, Y., and Haffner, P. Gradient-based learning applied to document recognition. In *Proceedings of the IEEE*, pp. 2278–2324, 1998.
- Liu, Y., Pagliardini, M., Chavdarova, T., and Stich, S. U. The peril of popular deep learning uncertainty estimation methods. *arXiv:2112.05000*, 2021.
- Lyu, C. and Liang, K. H. A unified gradient regularization family for adversarial examples. *arXiv:1511.06385*, 2015.
- Madry, A., Makelov, A., Schmidt, L., Tsipras, D., and Vladu, A. Towards deep learning models resistant to adversarial attacks. In *International Conference on Learning Representations*, 2018.
- Martín, E. S. and González, J. Bayesian identifiability : Contributions to an inconclusive debate. *Chilean journal of statistics*, pp. 69–91, 2010.
- Moran, G. E., Sridhar, D., Wang, Y., and Blei, D. M. Identifiable variational autoencoders via sparse decoding. *arXiv:2110.10804*, 2021.
- Nakkiran, P., Neyshabur, B., and Sedghi, H. The deep bootstrap framework: Good online learners are good offline generalizers. In *ICLR*, 2021.
- Neal, R. M. MCMC using Hamiltonian dynamics. In *Handbook of Markov Chain Monte Carlo*. Chapman & Hall/CRC, 2012.
- Netzer, Y., Wang, T., Coates, A., Bissacco, A., Wu, B., and Ng, A. Reading digits in natural images with unsupervised feature learning. 2011. URL <http://ufldl.stanford.edu/housenumbers/>.
- Neyshabur, B., Tomioka, R., and Srebro, N. In search of the real inductive bias: On the role of implicit regularization in deep learning. In *ICLR (Workshop)*, 2015.
- Ovadia, Y., Fertig, E., Ren, J., Nado, Z., Sculley, D., Nowozin, S., Dillon, J., Lakshminarayanan, B., and Snoek, J. Can you trust your model’s uncertainty? Evaluating predictive uncertainty under dataset shift. In *NeurIPS*, pp. 13991–14002, 2019.
- Pereyra, G., Tucker, G., Chorowski, J., Kaiser, L., and Hinton, G. E. Regularizing neural networks by penalizing confident output distributions. *arXiv:1701.06548*, 2017.
- Qin, Y., Wang, X., Beutel, A., and Chi, E. H. Improving calibration through the relationship with adversarial robustness. *arXiv:2006.16375*, 2021.
- Rasmussen, C. E. and Williams, C. K. I. *Gaussian Processes for Machine Learning (Adaptive Computation and Machine Learning)*. The MIT Press, 2005. ISBN 026218253X.
- Raue, A., Kreutz, C., Theis, F. J., and Timmer, J. Joining forces of bayesian and frequentist methodology: a study for inference in the presence of non-identifiability. *Philosophical Transactions of the Royal Society A: Mathematical, Physical and Engineering Sciences*, 371(1984), Feb 2013. ISSN 1471-2962. doi: 10.1098/rsta.2011.0544.

- Robbins, H. and Monro, S. A stochastic approximation method. *The Annals of Mathematical Statistics*, 1951.
- Rosca, M., Lakshminarayanan, B., Warde-Farley, D., and Mohamed, S. Variational approaches for auto-encoding generative adversarial networks, 2017.
- Shafahi, A., Saadatpanah, P., Zhu, C., Ghiasi, A., Studer, C., Jacobs, D., and Goldstein, T. Adversarially robust transfer learning. *arXiv:1905.08232*, 2020.
- Shah, H., Tamuly, K., Raghunathan, A., Jain, P., and Netrapalli, P. The pitfalls of simplicity bias in neural networks. In *Advances in Neural Information Processing Systems*, volume 33, 2020.
- Sokolic, J., Giryes, R., Sapiro, G., and Rodrigues, M. R. D. Robust large margin deep neural networks. *IEEE Transactions on Signal Processing*, 65:4265–4280, 2017. ISSN 1941-0476.
- Soudry, D., Hoffer, E., Nacson, M. S., Gunasekar, S., and Srebro, N. The implicit bias of gradient descent on separable data. *Journal of Machine Learning Research*, 19(70):1–57, 2018.
- Srivastava, N., Hinton, G., Krizhevsky, A., Sutskever, I., and Salakhutdinov, R. Dropout: A Simple Way to Prevent Neural Networks from Overfitting. *Journal of Machine Learning Research*, 15(56):1929–1958, 2014.
- Stutz, D., Hein, M., and Schiele, B. Disentangling adversarial robustness and generalization. In *CVPR*, pp. 6976–6987, 2019.
- Su, D., Zhang, H., Chen, H., Yi, J., Chen, P., and Gao, Y. Is robustness the cost of accuracy? - A comprehensive study on the robustness of 18 deep image classification models. In *ECCV*, 2018.
- Sun, B., Feng, J., and Saenko, K. Return of frustratingly easy domain adaptation. In *AAAI*, 2016.
- Szegedy, C., Zaremba, W., Sutskever, I., Bruna, J., Erhan, D., Goodfellow, I., and Fergus, R. Intriguing properties of neural networks. *arXiv:1312.6199*, 2014.
- Szegedy, C., Vanhoucke, V., Ioffe, S., Shlens, J., and Wojna, Z. Rethinking the inception architecture for computer vision. *arXiv:1512.00567*, 2015.
- Tramèr, F., Kurakin, A., Papernot, N., Goodfellow, I., Boneh, D., and McDaniel, P. Ensemble adversarial training: Attacks and defenses. In *ICLR*, 2018.
- Tsipras, D., Santurkar, S., Engstrom, L., Turner, A., and Madry, A. Robustness may be at odds with accuracy. *arXiv:1805.12152*, 2019.
- van Amersfoort, J., Smith, L., Teh, Y. W., and Gal, Y. Simple and scalable epistemic uncertainty estimation using a single deep deterministic neural network. In *ICML*, 2020.
- van Amersfoort, J., Smith, L., Jesson, A., Key, O., and Gal, Y. On feature collapse and deep kernel learning for single forward pass uncertainty. *arXiv:2102.11409*, 2021.
- Vapnik, V. N. *The nature of statistical learning theory*. Springer-Verlag New York, Inc., 1995. ISBN 0-387-94559-8.
- Wang, K., Gao, X., Zhao, Y., Li, X., Dou, D., and Xu, C.-Z. Pay attention to features, transfer learn faster cnns. In *ICLR*, 2020.
- Wang, Y. and Jordan, M. I. Desiderata for representation learning: A causal perspective. *arXiv:2109.03795*, 2021.
- Williams, R. J. and Peng, J. Function optimization using connectionist reinforcement learning algorithms. *Connection Science*, 3:241–268, 1991.
- Wilson, A. G., Hu, Z., Salakhutdinov, R., and Xing, E. P. Deep kernel learning, 2015.
- Wong, E., Rice, L., and Kolter, J. Z. Fast is better than free: Revisiting adversarial training. In *ICLR*, 2020.
- Xiao, H., Rasul, K., and Vollgraf, R. Fashion-MNIST: a novel image dataset for benchmarking machine learning algorithms. *arXiv:1708.07747*, 2017.
- Yosinski, J., Clune, J., Bengio, Y., and Lipson, H. How transferable are features in deep neural networks? In *NIPS*, 2014.
- Yuksel, O. K., Stich, S. U., Jaggi, M., and Chavdarova, T. Semantic perturbations with normalizing flows for improved generalization. In *ICCV*, 2021.
- Zhang, C., Bengio, S., Hardt, M., Recht, B., and Vinyals, O. Understanding deep learning requires rethinking generalization. In *ICLR*, 2017.
- Zhang, H., Yu, Y., Jiao, J., Xing, E. P., Ghaoui, L. E., and Jordan, M. I. Theoretically principled trade-off between robustness and accuracy. In *ICML*, pp. 7472–7482. PMLR, 2019.
- Zhang, J., Xu, X., Han, B., Niu, G., Cui, L., Sugiyama, M., and Kankanhalli, M. S. Attacks which do not kill training make adversarial learning stronger. In *ICML*, pp. 11278–11287. PMLR, 2020.

A. Extended Overview of Related Works and Discussions

The proposed method is inspired by several different lines of works, such as for example uncertainty estimation, works showing that low robustness of a data sample is correlated with high uncertainty estimate for that sample, training with input perturbations (or using these as a regularizer), among others. This section gives a brief overview of some relevant works, in addition to those listed in § 1 and 2 of the main paper.

A.1. Brief background on uncertainty estimation

In this section, we give an overview of the most popular uncertainty estimation (UE) methods.

Gaussian Processes (and extensions). As the gold-standard UE method is considered the Gaussian processes (GPs, [Rasmussen & Williams, 2005](#)) initially developed for regression tasks. GPs are a flexible Bayesian non-parametric models where the similarity between data points is encoded by a distance aware kernel function. More precisely, GPs model the similarity between data points with the kernel function, and use the Bayes rule to model a *distribution over functions* by maximizing the marginal likelihood ([Rasmussen & Williams, 2005](#)) of the Bayes formula. Thus, GPs require access to the full dataset at inference time. Accordingly, this family of methods and their approximations are computationally expensive and do not scale with the dimension of the data.

To use the advantages of both worlds: (i) the fast inference time of neural networks, and (ii) the good UE performances of GPs, a separate line of works focuses on combining neural networks with GPs. [van Amersfoort et al., 2020](#) combine Deep Kernel Learning ([Wilson et al., 2015](#)) framework and GPs by using NNs to learn low dimensional representation where the GP model is jointly trained, resulting in a method called *Deterministic Uncertainty Quantification* (DUQ). More recently, [van Amersfoort et al., 2021](#) showed that the DUQ method based on DKL *can* map OOD data close to training data samples, referred as “feature collapse”. The authors thus propose the *Deterministic Uncertainty Estimation* (DUE) which in addition to DUQ method ensures that the encoder mapping is bi-Lipschitz. It would be interesting to explore if these methods perform well on similar OOD experiments as those considered in this work. In App. D.4 we use the DUE model for UDP.

Bayesian Neural Networks (BNNs). BNNs are stochastic neural networks trained using a Bayesian approach. Following the same notation as in the main paper, given N training datapoints $\mathcal{D} = \{(\mathbf{x}_i, y_i)\}_{i=1}^N$, training BNNs extends to posterior inference by estimating the posterior distribution:

$$p(\boldsymbol{\omega}|\mathcal{D}) = \frac{p(\mathcal{D}|\boldsymbol{\omega})p(\boldsymbol{\omega})}{p(\mathcal{D})}, \quad (1)$$

where $p(\boldsymbol{\omega})$ denotes the prior distribution on a parameter vector $\boldsymbol{\omega} \in \Omega$. Given a new sample \mathbf{x}', y' , the predictive distribution is then:

$$p(y'|\mathbf{x}', \mathcal{D}) = \int_{\Omega} p(y'|\mathbf{x}', \boldsymbol{\omega})p(\boldsymbol{\omega}|\mathcal{D})d\boldsymbol{\omega}. \quad (2)$$

As GPs, BNNs are also often computationally expensive, what arises due to the above integration with respect to the whole parameter space Ω . The two most common approximate methods to train BNNs are (i) Mean-Field Variational Inference (MFVI, [Blei et al., 2017](#)), and (ii) Hamiltonian Monte Carlo (HMC, [Neal, 2012](#)), see ([Jospin et al., 2021](#)).

Ensembles & Monte Carlo Dropout (MCDropout). Popular epistemic UE method is *deep ensembles* ([Lakshminarayanan et al., 2017](#)), which trains a large number of models on the dataset and combines their predictions to estimate a predictive distribution over the weights. [Gal & Ghahramani, 2016](#) further argue that *Dropout* ([Srivastava et al., 2014](#)) when applied to a neural network approximates Bayesian inference of a Gaussian processes ([Rasmussen & Williams, 2005](#)). The proposed *Monte Carlo Dropout* (MC Dropout)—which applies Dropout at inference time—allows for a more computationally efficient uncertainty estimation relative to deep ensembles. [Ovadia et al.](#) further reduce the computational cost by applying Dropout only to the last layer.

A.2. Connecting robustness and simplicity bias with the margin of the model

[Vapnik \(1995\)](#) showed that the VC dimension—that measures the capacity of the model—of linear classifiers restricted to a particular data set can be bounded in terms of their margin, which measures how much they separate the data. [Elsayed et al.](#)

(2018) argue on the difference between the theory of large margin and deep networks, and a novel training loss to increase the margin of the classifier. Inspired by the fact that the training error of the neural networks is 0, recently (Nakkiran et al., 2021) empirically showed that “improved ideal-world accuracy is achieved by models which do not reduce the training loss too quickly”, where “ideal-world accuracy” refers to that of a having the infinite data-samples of the true generative model that generated the limited training samples. This is inline with our discussion in § 1 on the *simplicity bias*.

A.3. Adversarial training in input and in latent space

In the context of computer vision, small perturbations in image space that are not visible to the human eye can fool a well-performing classifier into making wrong predictions. However, further empirical studies showed that such training reduces the training accuracy, indicating the two objectives—robustness and generalization—are competing (Tsipras et al., 2019; Su et al., 2018). (Zhang et al., 2019) characterize this trade-off by decomposing the robust error as the sum of the natural error and the boundary error. They further introduce TRADES—see § 2, which adds a regularizer encouraging smoothness in the neighborhood of samples from the data distribution. Interestingly, both TRADES and UDP are unsupervised, in a sense that they do not rely on the label y_i of the starting data point x_i to obtain \tilde{x}_i . However, TRADES is orthogonal to UDP, as given a perturbation \tilde{x}_i it forces that the model’s output is smooth between \tilde{x}_i and x_i . Thus, given a perturbation obtained from UDP, the same method can be applied. We leave it as a future direction to further explore combining it with the herein proposed uncertainty driven perturbations. Wong et al. (2020) further pointed out a phenomenon referred to as *catastrophic overfitting* where the robustness of fast LDP methods rapidly drops to almost zero, within a *single* training epoch, and in § E.2 we provide results with UDP.

To improve the catastrophic overfitting of FGSM, Tramèr et al. (2018) propose adding a random vector ξ to FGSM as follows:

$$\delta_{R\text{-FGSM}} \triangleq \Pi_{\|\cdot\|_\infty \leq \epsilon} \left(\xi + \alpha \cdot \text{Sign} \left(\nabla_x \mathcal{L}(\mathcal{C}_\omega(x), y) \right) \right), \tag{R-FGSM}$$

where $\xi \sim U([-ε, ε]^d)$, $\alpha \in [0, 1]$ is selected step size, and Π is projection on the ℓ_∞ -ball.

Most similar to ours, (Zhang et al., 2020) argue that “friendly” attacks—attacks which limit the distance from the boundary when crossing it through early stopping—can yield competitive robustness. Their approach differs from ours as they do not consider the notion of uncertainty which also more elegantly handles the “manual” stopping.

Stutz et al. (2019) postulate that the observed drop in clean test accuracy appears because the adversarial perturbations leave the data-manifold, and that ‘on-manifold adversarial attacks’ will hurt less the clean test accuracy. The authors thus propose to use perturbations in the latent space of a VAE-GAN (Larsen et al., 2016; Rosca et al., 2017), and recently (Yuksel et al., 2021) used Normalizing Flows for this purpose due to their exactly reversible encoder-decoder structure. Our approach is orthogonal to these works as it can also be applied in latent space—see § 5.1.2, and interestingly, we show that our method does not decrease notably the clean test accuracy relative to common LDP methods, while it notably improves the model’s robustness relative to standard training.

A.4. Empirical results on the correlation between calibration and robustness

Recently, Qin et al., 2021 studied the connection between adversarial robustness and calibration, where the latter indicates if the model’s predicted confidence correlates well with the true likelihood of the model being correct (Guo et al., 2017). The authors find that the inputs for which the model is sensitive to small perturbations are more likely to have poorly calibrated predictions. To mitigate this, the authors propose an adaptive variant of label smoothing, where the smoothing parameter is determined based on the miscalibration, and the authors report that this method improves the calibration of the model even under distributional shifts. The above empirical observation on the correlation between the calibration and robustness motivates the proposed method here: using perturbations with poor calibration during training may improve both the robustness and calibration at inference.

A.5. Maximum entropy line of works

As one way to estimate the model’s uncertainty is using the entropy—see § 2, and moreover since we define a UDP variant that implements the UDP objective as a regularizer—Eq. UDPR, the approaches based on the *maximum entropy* principle (Jaynes, 1957) can be seen as relevant to ours. In particular, in the context of standard classification, Pereyra et al. (2017) penalize *confident* predictions by adding a regularizer that *maximizes* the entropy of the output distribution, since confident predictions

correspond to output distributions that have low entropy. Training is formulated as follows:

$$\min_{\omega} \mathbb{E}_{(\mathbf{x}, \mathbf{y}) \sim p_d} [\mathcal{L}(\mathcal{C}_{\omega}(\mathcal{E}(\mathbf{x}) + \delta), \mathbf{y}) - \gamma \cdot \mathcal{H}(\mathbf{x}, \omega)], \quad (\text{MaxE})$$

where $\mathcal{H}(\cdot)$ is defined in Eq. (E). [Pereyra et al.](#) point out that the above training procedure has connections with label smoothing ([Szegedy et al., 2015](#)) for uniform prior label distribution (see §3.2 of [Pereyra et al., 2017](#)), and the latter is also shown to improve the generalization. See also App. A.4 above that relates to label smoothing. Moreover, in the context of adversarial training, the results of ([Cubuk et al., 2017](#), §3.2) indicate that adding such a regularizer improves the model robustness to PGD attacks. While both UDPR and MaxE involve the maximum-entropy principle and modify the training objective with a regularizer, the difference is that UDPR uses the max-entropy principle to obtain the perturbations $\tilde{\mathbf{x}}$ of the input data points.

Entropy regularization is also widely used in reinforcement learning (RL) to improve the exploration by encouraging the policy to have an output distribution with high entropy ([Williams & Peng, 1991](#)). It remains an open interesting direction to find connections of UDP and the max-entropy principle in RL.

A.6. Discussion

The presented idea is connection between several lines of works, some of which are listed above. A high level summary of the above works is that: (i) the robustness to perturbations is tied to the value of the uncertainty estimate, (ii) epistemic uncertainty defines the objective we would like to target in training with perturbations, as we ultimately care about generalization and improving the margin of the classifier.

Finally, it is worth noting that uncertainty estimation for neural networks is an active line of research, since many popular methods fail to detect OOD data points ([Ovadia et al., 2019](#); [Liu et al., 2021](#)). However, such methods work well around the decision boundary, and we showed that this property is particularly useful, and it provides promising results for training with perturbations. Nonetheless, it remains an interesting direction to explore UDP with newly proposed UE methods.

B. Proof of Theorem 4.1

Recall that we consider a setting of binary classification $x \in \mathbb{R}$ data samples for simplicity, sampled from the data distribution p_d which is linearly separable, and each cluster has mean μ_1, μ_2 ($\mu_1 < \mu_2$), respectively, with label $y^{(1)} = -1$ and $y^{(2)} = +1$. For this problem, the optimal boundary is at $\omega^* = \frac{\mu_1 + \mu_2}{2}$. Since SGD yields the max-margin classifier for this setting (and so does regular training—see § 1), we consider a weaker requirement for the optimizer: at each iteration n , given data points $\tilde{x}_n^{(1)}$ and $\tilde{x}_n^{(2)}$, an oracle returns a *direction* $\tilde{\omega}_n$ that belongs in the interval between $\tilde{x}_n^{(1)}$ and $\tilde{x}_n^{(2)}$, that is:

$$\exists \alpha_n \in (0, 1), \quad \text{s.t.} \quad \tilde{\omega}_n = \alpha_n \tilde{x}_n^{(1)} + (1 - \alpha_n) \tilde{x}_n^{(2)}, \quad (\text{S1})$$

where we assume:

$$\alpha_n \sim \mathcal{U}(0, 1), \quad \text{i.e.} \quad \mathbb{E}[\alpha] = \frac{1}{2}, \quad (\text{A1})$$

Given ω_n and $\tilde{\omega}_n$, the update rule is as follows:

$$\omega_{n+1} = \omega_n + \eta(\tilde{\omega}_n - \omega_n), \quad (\text{S2})$$

where $\eta \in (0, 1)$ is the step-size.

Theorem B.1 (Convergence of UDP). *Given an oracle that takes as input two data points $\tilde{x}^{(1)}, \tilde{x}^{(2)}$ and returns a point that lies between these points sampled uniformly at random, the UDP method as per Alg. 1 converges to the max-margin classifier on a linearly separable dataset.*

Proof. Following Alg. 1, the UDP perturbations are described with:

$$\begin{aligned} \text{given } x_n^{(1)} \sim p_d(x|y = -1), \quad & \exists \beta_n \in (0, 1), \quad \text{s.t.} \quad \tilde{x}_n^{(1)} = \beta_n x_n^{(1)} + (1 - \beta_n) \omega_n \\ \text{given } x_n^{(2)} \sim p_d(x|y = 1), \quad & \exists \gamma_n \in (0, 1), \quad \text{s.t.} \quad \tilde{x}_n^{(2)} = \gamma_n x_n^{(2)} + (1 - \gamma_n) \omega_n, \end{aligned} \quad (\text{UDP-x})$$

where ω_n is the current iterate. Moreover, from Alg. 1 we have that $\mathbb{E}[\beta] = \frac{1}{2}$ and $\mathbb{E}[\gamma] = \frac{1}{2}$.

Given $x_1, x_2 \sim p_d$, and ω_n , we are interested in ω_{n+1} in expectation, and how it relates to the optimal max margin boundary $\omega^* = \frac{\mu_1 + \mu_2}{2}$. We have:

$$\begin{aligned} \mathbb{E}[\omega_{n+1} | \omega_n] &= \mathbb{E}[\omega_n + \eta(\tilde{\omega} - \omega_n) | \omega_n] \\ &= \omega_n + \eta(\mathbb{E}[\tilde{\omega}] - \omega_n) \\ &= (1 - \eta)\omega_n + \eta\mathbb{E}[\alpha\tilde{x}_n^{(1)} + (1 - \alpha)\tilde{x}_n^{(2)}] \\ &= (1 - \eta)\omega_n + \eta\mathbb{E}[\alpha(\beta x_n^{(1)} + (1 - \beta)\omega_n) + (1 - \alpha)(\gamma x_n^{(2)} + (1 - \gamma)\omega_n)] \\ &= (1 - \eta)\omega_n + \frac{\eta}{4}(\mu_1 + \omega_n + \mu_2 + \omega_n) \\ &= (1 - \frac{\eta}{2})\omega_n + \frac{\eta}{2}(\frac{\mu_1 + \mu_2}{2}) \\ &= (1 - \frac{\eta}{2})\omega_n + \frac{\eta}{2}\omega^*, \end{aligned}$$

where in fifth line we used (A1). Since $\eta \in (0, 1)$, in expectation ω_{n+1} lies on a line between ω_n and ω^* . This shows the boundary decision ω_n will have a tendency to move towards the optimal max margin boundary ω^* for $\eta \in (0, 1)$. \square

In the case of LDP-PGD, the position of the perturbations “ignores” the position of the boundary decision (it does not stop at it), as the loss is larger the further the perturbation moves following the direction from it to the decision boundary. Thus, for large $\epsilon > 1$ the perturbations will switch the label, and for $\epsilon = \infty$, the perturbations go to $\pm\infty$.

C. Pictorial Representation: UDP Vs. LDP

In Fig. 1 of the main paper we considered two samples per class, whose distances to the optimal decision boundary—denoted with ϵ_1 and ϵ_2 —largely differs, that is, we have $\epsilon_1 \ll \epsilon_2$. For completeness, in Fig. 6 we depict all the three cases: (i) $\epsilon_{train} \leq \epsilon_1$, (ii) $\epsilon_{train} \in (\epsilon_1, \epsilon_2)$, and (iii) $\epsilon_{train} \geq \epsilon_2$. While for the first case when $\epsilon_{train} < \epsilon_1$, UDP and LDP perturbations coincide, we observe that for the latter two these differ. UDP can be seen as it “locally adapts” the effective ϵ_i , making it less likely to cross the optimal decision boundary θ^* , avoiding training with a \tilde{x} whose label is semantically incorrect.

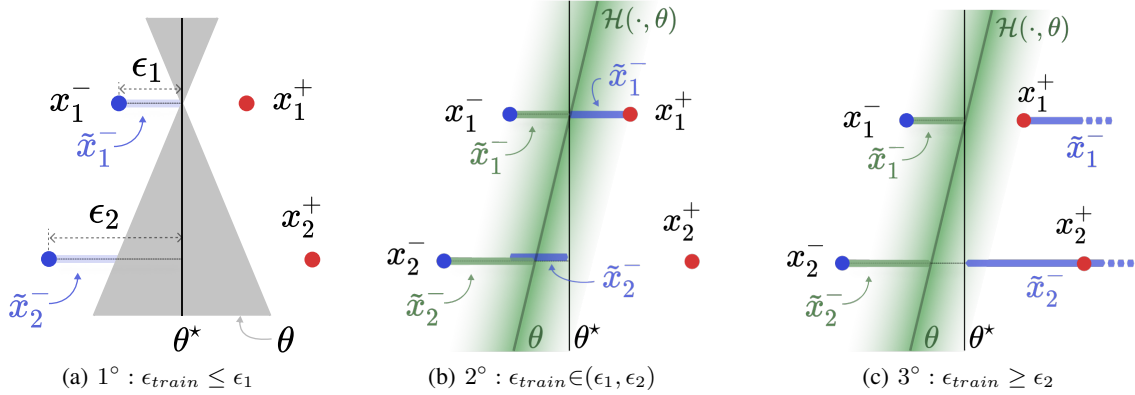


Figure 6: Complementary to Fig. 1—pictorial representations of LDP and UDP—where in contrast to Fig. 1 we depict the three cases: $\epsilon_{train} \leq \epsilon_1$, $\epsilon_{train} \in (\epsilon_1, \epsilon_2)$ and $\epsilon_{train} \geq \epsilon_2$. Circles represent training samples, and color their class $y \in \{-1, 1\}$. θ and θ^* denote the current decision boundary and the optimal one, resp. For clarity, only the perturbations \tilde{x}^- of the negative (blue) class are shown. **Fig. (a)**. Given *ideal* data-perturbation training procedure using $\epsilon_{train} < \epsilon$ the perturbed data points (either with UDP or LDP) will belong to the shaded blue area (assuming the boundary θ has 0 training loss). Thus, the final decision boundary will belong to the shaded grey area, and we *cannot* guarantee the margin is maximized—see § 1. **Fig. (b) and (c)**—explanation of *why UDP’s property of not crossing the boundary is advantageous*. The green shade depicts the uncertainty, where darker is higher – starting from a point with negative label the uncertainty increases, reaches its maximum, and then decreases. On the contrary, the loss used for LDP perturbations (of negative samples) keeps increasing the further we go on the right of θ . Thus, the LDP and UDP perturbed samples—obtained by iteratively following the direction that maximizes these quantities—differ, and their possible regions are shown in blue and green shade, resp., for different choices of $\epsilon_{train} > \epsilon_1$. When the perturbed samples from the negative class pass θ^* , LDP yields training pair (\tilde{x}_i^-, y_i) with a wrong label. This indicates that to avoid oscillations (caused by wrongly labeling input space regions), for LDP we are restricted to using $\epsilon_{train} \leq \epsilon$, but as Fig. (a) shows, this can be restrictive. On the other hand, for UDP we can have relatively larger ϵ which “locally adapts” and is effectively smaller in some region and larger in others. *Remark*: for easier comprehensiveness on the ϵ distances, we draw the perturbed samples region orthogonal to θ^* , whereas these are orthogonal to the current boundary θ .

D. Additional Results on Simulated Datasets

D.1. Max-margin decision boundary on the LMS-5 dataset

The maximum margin boundary for the LMS-5 dataset from §3 is shown in Fig. 7.

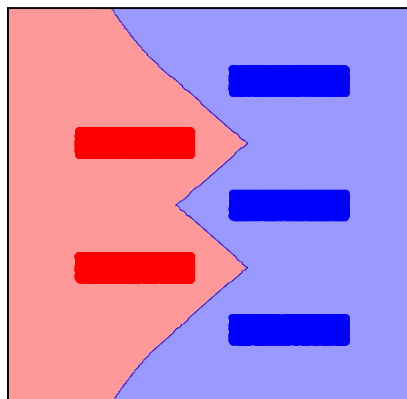


Figure 7: Complementary to Fig. 3 (bottom row): The boundary with the maximum margin on the LMS-5 dataset.

D.2. Simple dataset with two different distances

In the context of computer vision, adversarial training aims at finding “imperceptible” perturbation which does not change the label of the input data-point—see *AT-Asm*. Thus the selected ϵ value for training—herein denoted with ϵ_{train} —is typically small. In this work, we argue that satisfying *AT-Asm* “globally” can be in some cases very restrictive. As an additional simplified example to those presented in § 3, Fig. 8 depicts a toy experiment with non-isotropic distances between samples of opposite classes in \mathbb{R}^2 . In particular, there are two regions with notably different distances between samples from the opposite class, let us denote the respective optimal ϵ values for each region with ϵ_1 and ϵ_2 , and from Fig. 8, $\epsilon_1 \ll \epsilon_2$. In this section, we focus on *PGD*—top row, and below we discuss two *potential* issues of loss-based attacks.

AT-Asm enforces that we select $\epsilon_{train} = \epsilon_1$. In cases when $\epsilon_1 \ll \epsilon_2$ adversarial training only marginally improves the model’s robustness in the second region where ϵ_2 can be used locally during training as such perturbations will not modify the class label of samples of that region. Moreover, if the data is disproportionately concentrated—e.g. small mass of the ground truth data distribution is concentrated in the first region, and the remaining is concentrated in the second region—one still needs to select $\epsilon_{train} = \epsilon_1$, as per *AT-Asm*.

To later contrast the behavior of loss-based *PGD* with uncertainty-based *PGD*, in Fig. 8(e)-8(b) we consider loss-based *PGD* with ϵ_{train} which *violates AT-Asm* (thus this value would not be used in practice by practitioners). From Fig. 8 we observe that *PGD* can perturb the sample by moving it on the opposite side of the boundary—resulting in *mislabeled* samples. See Fig. 15 for such analysis on CIFAR-10. While Fig. 8(e)-(b) illustrates the difference between attacks for a *fixed model*, Fig. 8(c) illustrates the decision boundaries *after* adversarial training with *PGD*. Similarly, Fig. 8(d) shows that for this “violating” case *PGD* training is characterized with large oscillations of the decision boundary, resulting in inefficient training. See App. D.4 for results on the same dataset but using Gaussian Process as a model.

In the general case, the largest ϵ value which does not break the *AT-Asm* assumption *locally* would *differ* among m non-overlapping local regions of the input data space, and let us denote these with $\epsilon_1, \epsilon_2, \dots, \epsilon_m$. Note that, as such none of the $\epsilon_i, i \in 1, \dots, m$ when applied to the corresponding i -th region changes the label class. Let without loss of generality $\epsilon_1 < \epsilon_2 < \dots < \epsilon_m$. *AT-Asm* forces that for training we select $\epsilon_{train} = \min(\epsilon_1, \epsilon_2, \dots, \epsilon_m) = \epsilon_1$. The decision boundary of a model f trained adversarially with ϵ_{train} lies within a margin that is far by *at least* $\frac{\epsilon_{train}}{2}$ from any training data point.

On the other hand, *UDP* achieves the above desired goal in an elegant way: as *UDP* does not cross the decision boundary, it effectively uses varying $\epsilon_i \leq \epsilon_{train}$, for different local regions of the input data space, where ϵ_{train} is selected beforehand. From Fig. 8, we observe that *UDP*-based training or more precisely *UDP-PGD* is relatively less sensitive to the choice of ϵ_{train} . Importantly, inline with the above discussion, using large ϵ for *UDP-PGD* during training does not deteriorate its final clean accuracy, as Fig. 8(c) depicts. Finally, from Fig. 8(d) we observe that even for large selected values of

ϵ_{train} —which value breaks **AT-Asm** solely *globally*, the boundary decision of **UDP** training oscillates relatively less to that of **PGD** and mostly close to the ground-truth decision boundary. By being able to use larger values for ϵ , **UDP** allows for larger “exploration” of the input space and in turn learn “better” latent representations and decision boundary, characterized by better clean-accuracy and **PGD** robustness trade-off, as we shall see in § 5. This is in sharp contrast to **PGD**, which is forced to use the smallest ϵ_1 even in cases when $\epsilon_1 \ll \epsilon_m$, as using ϵ_{train} value which violates **AT-Asm** performs poorly. Moreover, we argue that such non-isotropic margins as in Fig. 8 are more likely to occur in real-world datasets.

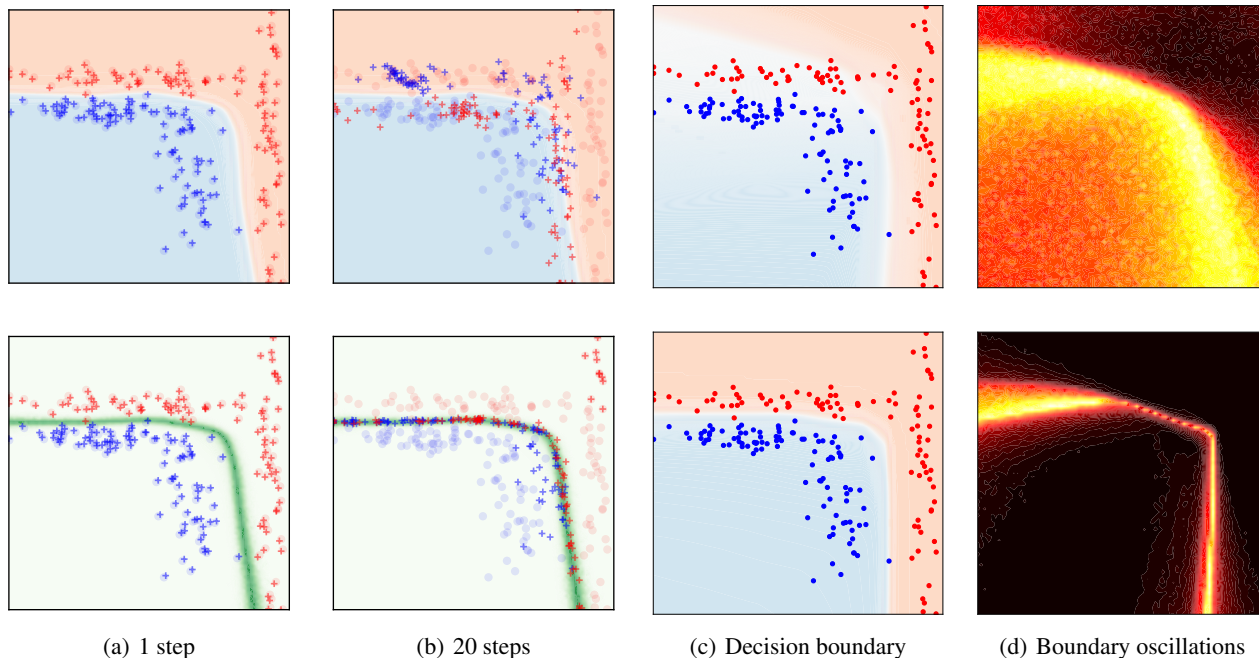


Figure 8: 2D experiment—performance of **LDP-PGD** (left) Vs. **UDP-PGD** (right) using ϵ which *violates* the **AT-Asm**. **Columns (e)-(b)**. Attacks to a *fixed trained classifier*, with 1 and 20 steps (columns), resp. \circ and $+$ depict the clean and perturbed samples, resp., and their color blue/red depicts their class. **Top row**: background depicts the assigned probability to each class of the attacked model, including its decision boundary. **Bottom row**: background depicts the uncertainty estimates of a 10 model ensemble, where darker green is higher. **Column (c)**. Decision boundaries *after* adversarial training with *large* ϵ (and $k = 15$, $\alpha = 0.05$). **Column (d)**. Summary of the boundary oscillations over the updates, for a fixed mini-batch size for both **PGD** and **UDP**. For each point $x \in \mathbb{R}^2$ we count how many times the classifier changed its prediction, and depict with darker to lighter color zero to many changes, resp. See App. D.2 for discussion.

D.3. Additional results on the *Narrow Corridor* dataset

Fig. 9 is complementary to that of Fig. 3, and shows the methods’ performance for varying ϵ values.

D.4. UDP with Gaussian Process-based model

In this section, we consider additional uncertainty estimation methods, and we show that **UDP** can be implemented with these too. As an uncertainty estimation model we use Gaussian Processes, which are considered a the gold standard in uncertainty estimation, see details in App. A. In particular, we use the *Deterministic Uncertainty Estimation* (DUE) method (van Amersfoort et al., 2021). This method aims at estimating epistemic uncertainty using a single forward pass through the network by exploiting Gaussian Processes applied to deep architectures (Wilson et al., 2015). We choose this particular method because it is known to give higher uncertainty estimates to outliers relative to other popular methods (see Fig. 1 van Amersfoort et al., 2021).

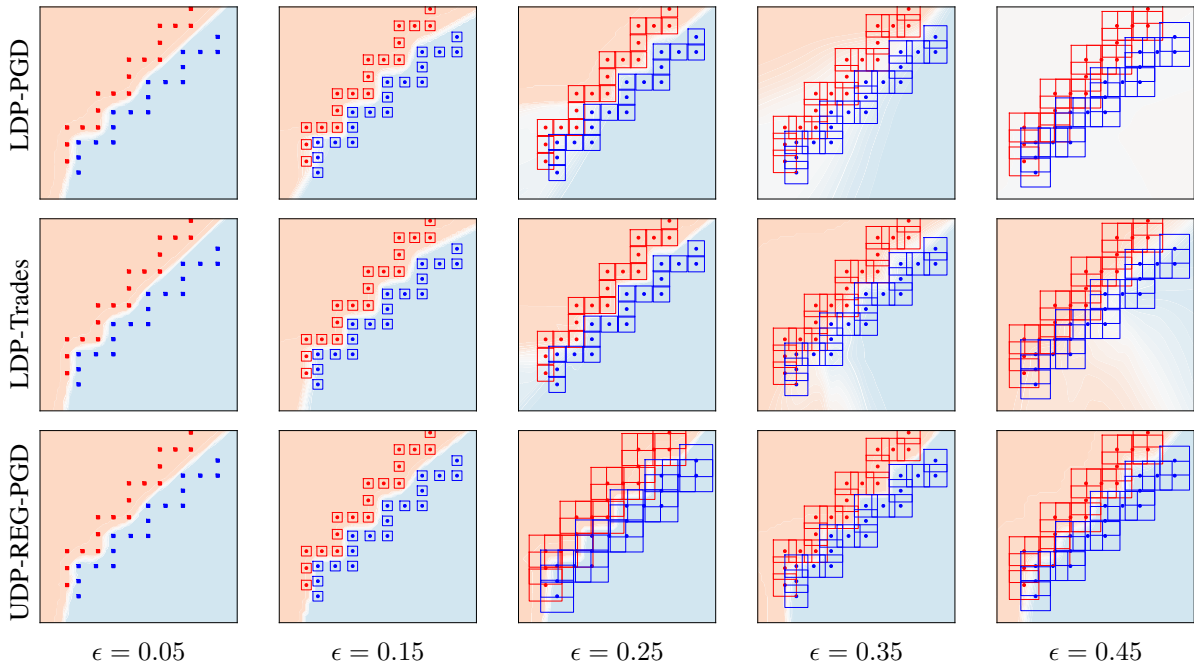


Figure 9: Complementary results to that in Fig. 3, for varying $\epsilon \in 0.05, 0.15, 0.25, 0.35, 0.45$. The hyperparameters step size and number of steps are fixed for all methods to $\alpha = 0.05$, and $k = 10$

D.5. Visualizations of the PGD and UDP Perturbations

In this section, we first train a model using DUE on the clean (unperturbed) 2D dataset, and then we depict the different attacks.

In Fig. 10 we can see the decision boundary and the uncertainty, measured in terms of entropy of the model in classifying the clean dataset (without adversarial training). In this case, as in 3, we observe that while the PGD-50 samples cross notably the boundary, the UDP perturbations do not. Moreover, UDP perturbations push the samples both towards the decision boundary and towards unexplored regions of the dataset. Both the PGD and UDP perturbations are applied using $\epsilon = 1$ and $\alpha = 0.1$.

D.6. Adversarial Training using the DUE Classifier

In this section, we use the same setup as in the previous section, however, we train adversarially the DUE model using PGD and UDP perturbations. For both PGD and UDP we use: $\epsilon = 1$ and $\alpha = 0.1$.

Fig. 11 depicts the results. We observe that PGD training led to a very different decision boundary compared to the one obtained by training only with clean samples and leads to a model that is not able to classify the dataset with good performances. On the other hand, UDP-PGD preserves a good decision boundary, very similar to the one shown in Figure 10.

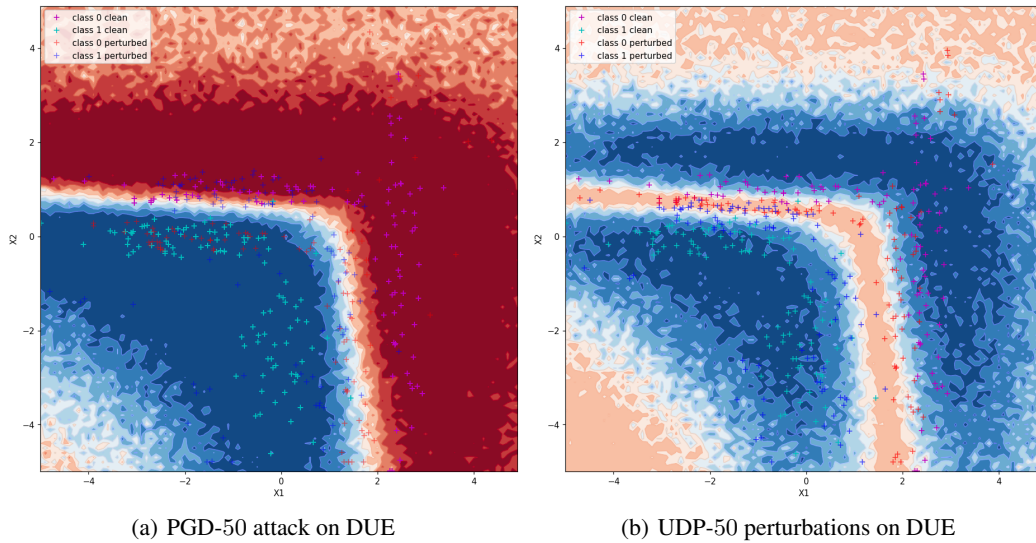


Figure 10: PGD and UDP attacks on a *fixed* DUE (van Amersfoort et al., 2021) model trained solely with clean data on the toy example from § 3. Light and dark blue crosses denote clean and perturbed samples of class 1, and similarly, pink and red crosses denote clean and perturbed samples of class 0. **Left:** the background depicts the loss landscape of the model (and its decision boundary), clean dataset and perturbed samples using the PGD-50 attack. Note how the PGD samples cross the boundary and go to the other class’ region. **Right:** entropy of the model, clean dataset and UDP-50 perturbed samples. UDP samples do not cross the boundary and are able to go towards unexplored regions of the dataset.

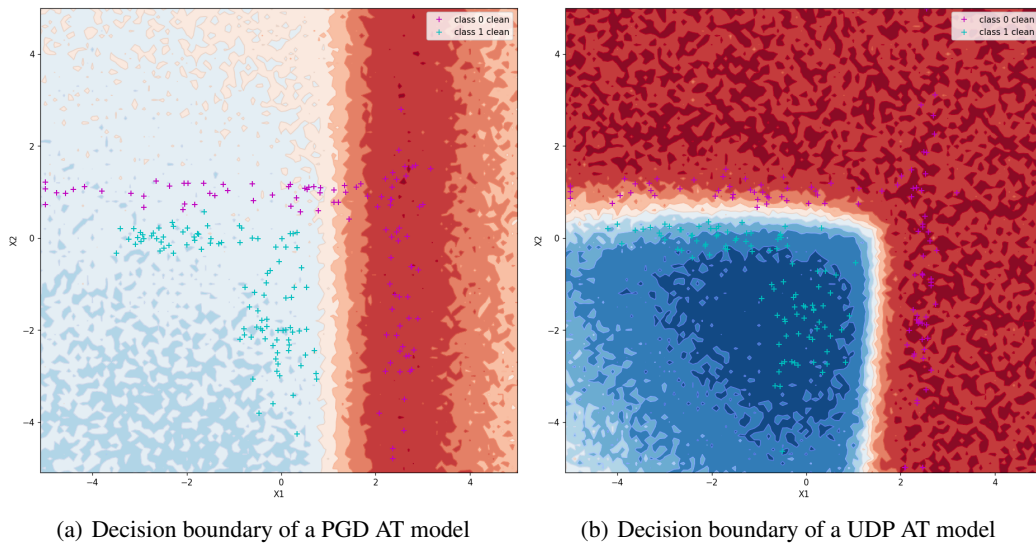


Figure 11: PGD and UDP-PGD on a DUE model trained on a non-isotropic toy example dataset. **Left:** decision boundary obtained by training adversarially with PGD-50 perturbed samples. The model is not able to correctly classify the dataset. **Right:** decision boundary obtained by training adversarially with UDP-50 perturbed samples. The model is not is now able to classify correctly the dataset and the decision boudnary is much more similar to the one obtained by training with clean samples only (shown in Figure 10).

E. Additional Results on Real-world datasets

E.1. Omitted Results

In addition to Fig. 4 of the main paper, Fig. 12 depicts the clean test accuracy for **Fashion-MNIST**.

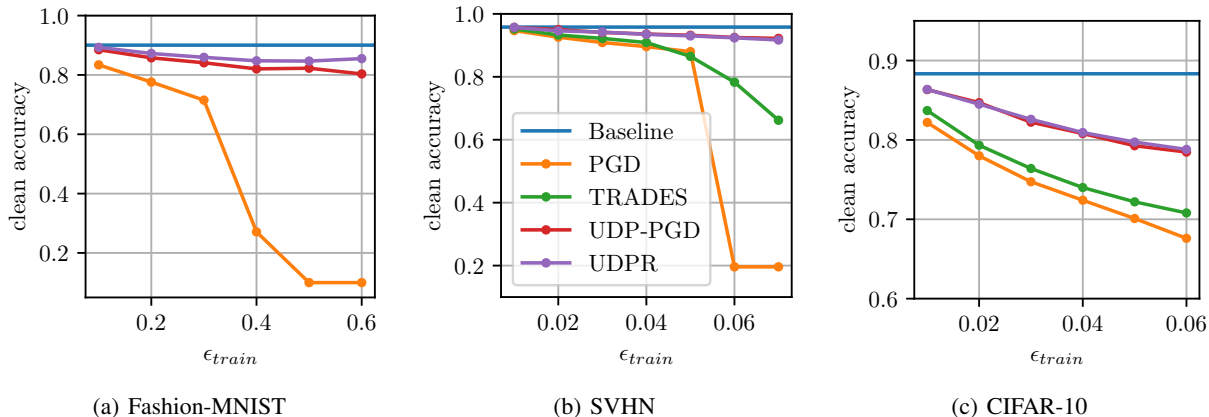


Figure 12: Complementary figure to that of Fig. 4 that includes **Fashion-MNIST**: *Clean accuracy* (y -axis) comparison between PGD, TRADES, UDP-PGD, and UDPR, for varying ϵ_{train} used for training (x -axis). Results are averaged over multiple runs.

E.2. Catastrophic overfitting

Fashion-MNIST. We used a LeNet model trained on the Fashion-MNIST dataset. Both for FGSM and UDP-PGD *with one step* we used during training $\epsilon = 0.2$ and $\alpha = \epsilon$; and for testing we used PGD with 20 iterations, $\epsilon = 0.2$ and $\alpha = 0.01$. See App. F for further details.

CIFAR-10. For the experiments on CIFAR-10 we used UDP combined with an ensemble of five-models sampled with MC Dropout, using a ResNet-18 (He et al., 2016) architecture, see App. F for details.

Results. Fig. 13(a) and 13(b) depict the results on FashionMNIST which evaluate if the methods are prone to Catastrophic Overfitting (CO). Relative to FGSM, single model UDP notably improves CO, as although there is a downward trend in PGD-20 accuracy after a certain number of iterations, it does not reduce to 0.

E.3. Visual Appearance of the Attacks

In Fig. 15 we use large ϵ -ball to obtain clearly visible difference between the PGD and UDP-PGD attacks, as well as to see if the insights from the experiment from Fig. 8, § 3 could extend to real world setups. The topmost row depicts clean samples from CIFAR-10. Using an already trained classifier on CIFAR-10, we show how UDP and PGD perturbations look, in the middle and bottom rows, respectively. We observe that for large ϵ -ball PGD attacks *can* make the content non-recognizable for human eye, whereas the class of UDP perturbed samples remains perceptible.

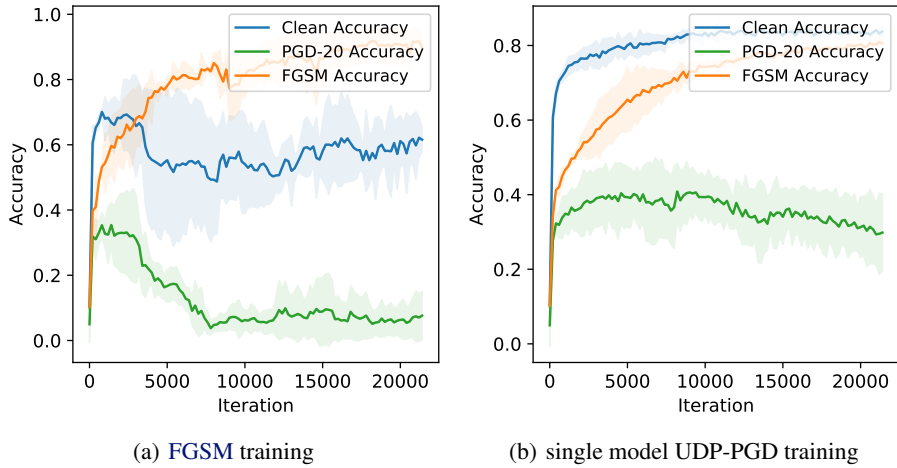


Figure 13: Catastrophic Overfitting (CO) on the **FashionMNIST** dataset using a LeNet model; results are averaged over 3 runs. **Left:** training with FGSM using a step size $\alpha = 0.2$, $\epsilon = \alpha$; and testing against PGD-20 with $\epsilon = 0.2$ and $\alpha = 0.01$. Soon after the beginning of the training the FGSM accuracy suddenly jumps to very high values while the PGD-20 accuracy approaches 0. Note also how the clean accuracy decreases and becomes lower than FGSM after CO. **Right:** training with UDP-PGD (with 1 single step) using a step size $\alpha = 0.2$, $\epsilon = \alpha$; and testing against PGD-20 with $\epsilon = 0.2$ and $\alpha = 0.01$. While the PGD robustness for UDP-PGD decreases to some extent, the drop is not as large as for FGSM AT. Note also how training with UDP-PGD with a single step leads to higher clean accuracy.

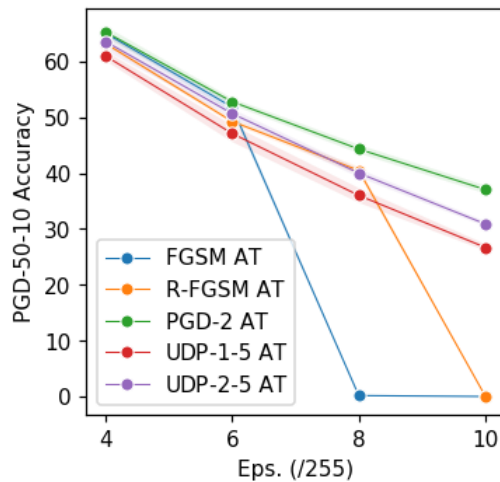


Figure 14: *Catastrophic overfitting* (CO) on **CIFAR-10** using ResNet 18, averaged over 3 runs. PGD robustness (50 iterations, 10 restarts) evaluated for multiple ϵ_{test} for FGSM, Random-FGSM, PGD with two steps, UDP-PGD with 1 step and an ensemble of 5 models, and UDP-PGD with 2 steps and an ensemble of 5 models.

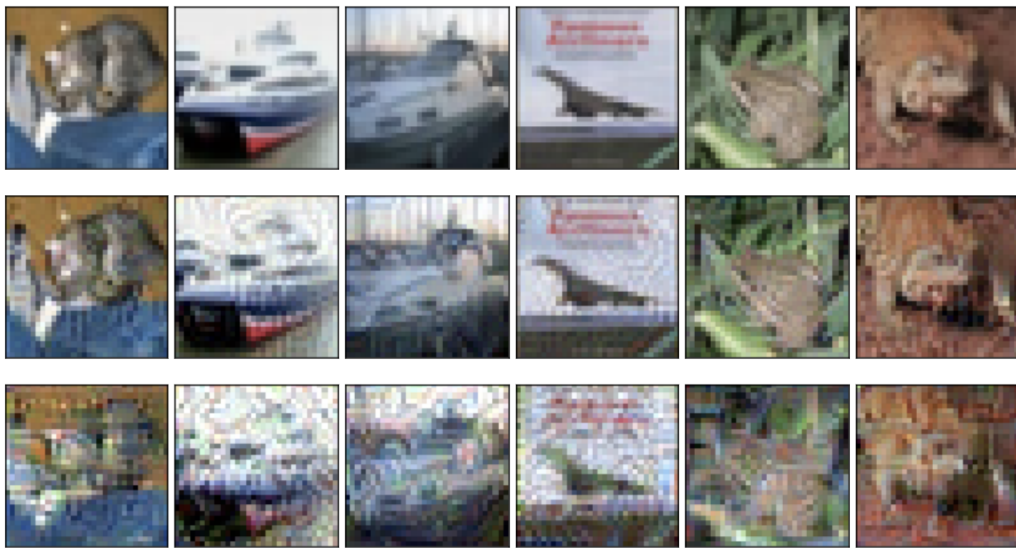


Figure 15: Illustration of the difference between PGD and UDP perturbations for a classifier trained on CIFAR-10: (i) top row: clean samples, (ii) middle row: UDP perturbations, (iii) bottom row: PGD attacks, where for UDP and PGD we use same setup (1000 steps, step size of 0.001, $\epsilon = \infty$). We use large number of steps to verify empirically if the difference between UDP and PGD depicted in Fig. 8 holds on real-world datasets as well. Contrary to the PGD-perturbed samples, the correct class of the UDP-perturbed ones remains perceptible. See § E.3.

F. Details on the implementation

Source code. Our source code is provided in this anonymous repository: github.com/mpagli/Uncertainty-Driven-Perturbations

For completeness, in this section we list the details of the implementation.

F.1. Architectures & Hyperparameters

In this section, we describe in detail the architecture used for our experiments for the various datasets.

F.1.1. ARCHITECTURE FOR EXPERIMENTS ON FASHION-MNIST

FashionMNIST. We used a LeNet architecture as described in table 6. This network has been trained for 100 epochs using the Adam optimizer (Kingma & Ba, 2015) with a learning rate of 0.001. The parameters of the models are initialized using PyTorch default initialization.

LeNet
<i>Input: $x \in \mathbb{R}^{28 \times 28}$</i>
conv. (kernel: 5×5 , $1 \rightarrow 6$; padding: 2; stride: 1)
ReLU
max pooling (kernel: 2×2 ; stride: 2)
convolutional (kernel: 5×5 , $6 \rightarrow 16$; stride: 1)
ReLU
max pooling (kernel: 2×2 ; stride: 2)
Flattening
fully connected ($16 \times 5 \times 5 \rightarrow 120$)
ReLU
fully connected ($120 \rightarrow 84$)
ReLU
fully connected ($84 \rightarrow 10$)
<i>Softmax(\cdot)</i>

Table 6: LeNet architecture used for experiments on **FashionMNIST**. With $h \times w$ we denote the kernel size. With $c_{in} \rightarrow y_{out}$ we denote the number of channels of the input and output, for the convolution layers, and the number of input and output units for fully connected layers.

F.1.2. ARCHITECTURE FOR EXPERIMENTS ON CIFAR-10 AND SVHN

The ResNet-18 setup on CIFAR-10 and SVHN is as in (Andriushchenko & Flammarion, 2020). We trained for 60 epochs with a triangular learning rate scheduler and a peak learning rate of 0.15. For the experiments in Sec.5.2 we trained for 100 epochs with a triangular learning rate scheduler and peak learning rate of 0.05. For both settings we use the SGD optimizer with a batch size of 256.

Solely for some of the experiments in the appendix—see App.E.2, we modified the original ResNet architecture to accommodate the MC-dropout sampling procedure, see Tab. 7. The modification consists of adding a dropout layer with dropout probability $p = 0.2$ after each convolutional layer.

F.2. Increasingly larger model capacity experiments

Although relatively less than LDP, we observe that when the robustness is improved, the clean test accuracy decreases for UDP too. Since the “complexity” of the dataset increases with training samples perturbations and while doing so we keep the same models that are used for the (clean) unperturbed dataset, a question arises if this decrease is due to insufficient model capacity. As in (Madry et al., 2018) we run experiments with increasingly larger model capacity on Fashion-MNIST. In particular, we keep the same architecture—in this case LeNet (Lecun et al., 1998), but we increase the number of filters in the two convolutional layers and in the first fully connected layers. This is done via a multiplicative parameter. We tested

ResBlock (part of the ℓ -th layer)	ResNet Classifier
<i>Bypass:</i> conv. (ker: 1×1 , $64 \rightarrow 64 \times \ell$; str: 2; pad: 1), if $\ell \neq 1$ Batch Normalization, if $\ell \neq 1$ <i>Feedforward:</i> conv. (ker: 3×3 , $64 \rightarrow 64 \times \ell$; str: $1_{\ell=1}/2_{\ell \neq 1}$; pad: 1) Batch Normalization <i>ReLU</i> MCD ($p = 0.2$) conv. (ker: 3×3 , $64 \times \ell \rightarrow 64 \times \ell$; str: 1; pad: 1) Batch Normalization <i>Feedforward + Bypass</i> <i>ReLU</i> MCD ($p = 0.2$)	Input: $x \in \mathbb{R}^{3 \times 32 \times 32}$ conv. (ker: 3×3 ; $3 \rightarrow 64$; str: 1; pad: 1) Batch Normalization <i>ReLU</i> MCD ($p = 0.2$) $3 \times \text{ResBlock} (\ell = 1)$ $6 \times \text{ResBlock} (\ell \in [2, 3, 4])$ <i>ReLU</i> AvgPool (ker: 4×4) Linear($512 \rightarrow 10$)

Table 7: ResNet architectures for the experiments on catastrophic overfitting trained on **CIFAR-10**. Each ResNet block contains skip connection (bypass), and a sequence of convolutional layers, normalization, and the ReLU non-linearity. For clarity we list the layers sequentially, however, note that the bypass layers operate in parallel with the layers denoted as “feedforward” (He et al., 2016). The ResNet block for the model (right) differs if it is the first block in the network (following the input to the model).

with values of this parameter ranging from 2 to 12.